Fall 2016

Shear behavior of reinforced fly ash-based geopolymer concrete

Noor S. Yacob

Department:

SHEAR BEHAVIOR OF REINFORCED FLY ASH-BASED GEOPOLYMER CONCRETE

by

NOOR S. YACOB

A THESIS

Presented to the Graduate Faculty of the

MISSOURI UNIVERSITY OF SCIENCE AND TECHNOLOGY

In Partial Fulfillment of the Requirements for the Degree

MASTER OF SCIENCE IN CIVIL ENGINEERING

2016

Approved by

Mohamed A. ElGawady, Advisor
John J. Myers
Lesley H. Sneed
Aly M. Said

PUBLICATION THESIS OPTION

This thesis has been prepared in the style such that the individual paper section, (i.e., pages from 15 to 56) will be submitted for publication in the Journal of *Construction and Building Materials*, an international journal dedicated to the investigation and innovative use of materials in construction and repair.

ABSTRACT

The geopolymerisation of aluminosilicate materials such as fly ash has been a radical change in construction material's chemistry and composition, compared to the portland cement-based concrete calcium silicate-hydrate chemistry. The adoption of fly ash in concrete industry is a good use of by-product ashes to reduce emissions of the greenhouse gas implicitly. However, in this research, the replacement of portland cement by fly ash is 100%, which makes it a zero-cement concrete with no proprietary chemical additives.

Geopolymer concrete (GC) is a revolutionary synthetic material that combines sustainability and high engineering properties, and it is relatively cost-effective compared to portland cement-based concrete, its traditional competitor. Limited research on the structural performance of GC versus the microstructural and material properties has been conducted until now, thus this research focuses on the shear behavior of fly ash-based geopolymer concrete. The main three factors that affect the shear strength are dowel action, shear reinforcement ratio, and shear span-to-effective depth ratio. The experimental program consists of six beams: one Conventional Concrete (CC) beam and five Geopolymer Concrete (GC) beams. Two beams had no stirrups and different flexural reinforcement ratio (ρ_w), two beams had different shear reinforcement ratio (different stirrup spacing, s) and one beam had higher shear span-to-effective depth ratio (a/d). All the beams failed in shear except two beams; one had higher a/d ratio and one had smaller s. These beams failed in flexural-shear mode. All the GC beams showed high shear strength.

ACKNOWLEDGMENTS

I am so grateful and proud to have such an amazing advisor like Dr. Mohamed ElGawady, he is an outstanding professor and excellent researcher. I thank him for all that he taught me and for the encouragement and support he has provided through my work.

I would like to express my sincere gratitude to my dear husband that without his support and help, this research would not be possible. Also I owe much to my lovely children who were so patient and proud of what I was doing. Also, I would like to thank all my family members and friends who were a great support.

Special thanks to my advisory committee members, Dr. John J. Myers, Dr. Lesley H. Sneed, Dr. Aly M. Said for their time to review this document.

My great thanks to my wonderful team members Ahmed Gheni, Sujith Anumolu, Mohanad Abdulazeez, Ayman Moustafa, Song Wang, and my colleagues Hayder Alghazali, Zena AlJazaeri, Zuhair Aljabiri, and Meyyada Abdulhady.

My sincere appreciation to Gary Abbott, John Bullock, Jason Cox, Michael Lusher, Brian Swift for their technical assistance. Also, many thanks to Dr. Soo Duck Hwang.

Last but not least, I would like to thank James Oquin from Boral Technologies and Stephanie Rose form PQ Corporation for their great help to provide the material for this research.

TABLE OF CONTENTS

LIST OF ILLUSTRATIONS

Page

SECTION

PAPER I

LIST OF TABLES

Page

PAPER I

NOMENCLATURE

Symbol	Description
A_s	Area of longitudinal reinforcement
A_v	Steel vertical reinforcement area
$A_{v,min}$	Minimum shear reinforcement area
a	Shear span
a_g	Aggregate size (AASHTO LRFD, 2004)
a/d	Shear span-to-depth ratio
b	Width of cross-section
b_v	Effective width of cross-section
b_w	Width of cross-section or width of web
d	Effective depth of cross-section
d_v	Effective shear depth
$\Delta_{sd1}, \Delta_{sd2}$	Measured diagonals of the deformed truss unit due to shear and flexure deformation.
Δ_{s1}, Δ_{s2}	Diagonals of the deformed truss unit due to pure shear deformation
E_c	Modulus of elasticity of the concrete
E_s	Modulus of elasticity of the steel
f'_c	Compressive strength of the concrete
f_t	Splitting tensile strength of the concrete
f_y	Yield stress of steel
f_{yt}	Yield stress of transverse steel reinforcement

h	Height of cress-section, and height of the truss unit (Jirawattanasomkul 2013)
l	Length of the truss unit (Jirawattanasomkul, 2013)
L	Length of the beam
M_n	Nominal moment capacity
M_u	Factored shear moment
P	Maximum load at failure
s	Center-to-center spacing of steel stirrups
$x_1 \; and \; x_2$	Horizontal displacements of the top and bottom truss unit cords due to shear and flexure deformation
V	External shear force
V_c	Concrete contribution to shear strength
V_s	Steel contribution to shear strength
V_{test}	Experimentally determined total shear resistance
V_u	Factored shear force
v	Shear stress
β	Factor indicates the ability of diagonally cracked concrete to transmit tension
γ	Principle shear strain
y_f	Vertical displacement due to flexure deformation
y_s	Vertical displacement due to shear deformation
$\delta_1 \; and \; \delta_2$	Principle displacements in concrete due to diagonal crack
ε_c	Compressive strain in the concrete
ε_s	Strain in tension reinforcement
ε_x	Longitudinal strain in the web

θ	Shear crack angle
θ_{sd}	Rotation of the cross-section plane due to shear and flexure deformation
ρ_b	Balanced reinforcement ratio;
ρ_{min}	Minimum flexural reinforcement ratio; and
ρ_w	Ratio of A_s to $b_w d$.

1. INTRODUCTION

1.1. BACKGROUND

Cement is the most widely used manufactured material in the world. It is the essential ingredient of concrete production. In the past decades, numerous studies have been conducted to proportionally replace cement in concrete with waste material and industrial by-products such as fly ash (FA) and ground granulated blast furnace slag (GGBS) which reduces the greenhouse gas footprint associated with the cement manufacturing. Furthermore, using waste and industrial by-product materials will reduce the consumption of the non-renewable natural resources in construction creating more sustainable concrete. Utilizing fly ash in the concrete industry has not only been a good impact on the environment but also improves the durability and economy of concrete production. However, most of past studies limit the use of the supplementary cementitious materials to about 30% of the cement content.

Fly ash-based geopolymer concrete is a radical change in construction material and concrete industry where no Portland cement is used and 100% of the cementitious material is industrial by-product, i.e., fly ash. The adoption of fly ash-based concrete is a good use of the massive fly ash land fill across the world resulting from the coal combustion power plants.

A review of previously published work indicates that very few studies have addressed the structural behavior of fly ash-based geopolymer concrete. This project intends to investigate the shear behavior of fly-ash based geopolymer reinforced concrete beams.

1.2. OBJECTIVE AND SCOPE OF WORK

The basic objective of this research study was to evaluate the shear behavior of geopolymer concrete (GC) beams and the suitability of the available standards and shear provisions of conventional concrete to determine the shear strength of GC and compare it with the experimental results. The mix design used in this research consists of class F fly ash as the only cementitious material. The fly ash was activated by sodium hydroxide and sodium silicate liquids under moderate temperature for one day applied to the freshly casted concrete. Two types of silicate liquids having different concentrations were used in the trail mixtures, it was found that a minimal decrease in the concentration of silicate solids does not affect the compressive strength significantly.

The thesis's objective was achieved through the following tasks: (1) review of applicable literature about shear behavior of conventional concrete, and material properties of GC; (2) conduct a series of trial mixtures to reach to the target strength of GC; (3) investigate the fresh and hardened properties of the developed GC following the appropriate ASTM specifications; (4) study the effect of curing time on the polymerization reaction rate; (5) design, construct, test, and analyze data of six beam specimens; (6) compare the shear strengths of the investigated beams to those obtained from different design standards; (7) measure the shear deformation and average principle shear strain of GC and compare them to those of conventional concrete; (8) summarize findings and develop conclusions and recommendations.

1.3. THESIS OUTLINE

This thesis includes three sections and seven appendices. The first section gives a brief introduction to the subject area and explains the need for the current research study.

The section presents also the objective and the scope of work of the study, as well as the literature review to establish the state of art of the proposed topic and information about the previous work done in related fields.

The second section presents a journal paper discussing the shear response of GC.

The third section summarizes the findings and conclusions of the study and proposes future research.

The appendices include the trial mixtures tables, chemical composition of Class F fly ash that been used in the research, curves of the strain gauges and LVDTs readings vs. strength of the tested beams, thermocouple readings during the heat curing of the freshly casted beams, and the provisions and notations of the available international codes about shear, that been used to evaluate the shear strength of the tested beams.

2. LITERATURE REVIEW

The purpose of this section is to review the previous work on geopolymer concrete with particular attention to the material properties and its structural behavior.

2.1. MATERIAL PROPERTIES

The material properties of geopolymer concrete affected by different parameters, these parameters include, but not limited to the following:

2.1.1. Cementitious Binder. The Cementitious binder in geopolymer concrete is alkaline-activated material that is rich in alumina and silica found as industrial by-products such as fly ash, blast furnace slag, rice husk, metakaolin, and red mud, or natural minerals such as pozzolans (Aydin and Baradan 2012). Among the waste or by-product materials, fly ash class F or (low-calcium fly ash) and slag are the most potential source of geopolymers (Wallah and Rangan 2006). However, other types of fly ash, such as class C fly ash (or high-calcium fly ash), has been studied as a binder in GC. The calcium content, generally, considered as a contaminant, producing different chemical assemblage that may cause lower strength and lower reaction rate (Li et al 2013). On the other hand, some studies concluded that class C fly ash, influenced the fresh and hardened properties of GC, and lead to the formation of calcium silicate hydrate (C-S-H) plus the geopolymer products, that, as the fraction of calcium silicate glass increases, the setting time decreases, and the compressive strength increases (Diaz et al. 2010). It was found that the highest strengths of paste and mortar of class C fly ash-based geopolymer were when the specimens cured at 70°C (158°F) for 24 hours (Li et al. 2013).

2.1.2. Aggregate Content. Based on a study carried out by Joseph and Mathew (2012) on the influence of aggregate content on the engineering properties of GC, it was

observed that the compressive strength of GC increased with the increase in total aggregate content up to 70% of the mix by volume and then it decreased. Also, it was observed that the compressive strength of GC increased when the ratio of fine aggregate-to-total aggregate increased up to 35%, and beyond this ratio, the strength decreased. This was similar to conventional concrete, because the optimum proportion of fine aggregate and coarse aggregate yields efficient binding by the concrete paste.

2.1.3. Curing Effect. Sanni and Khadiranaikar (2013) presented a study on the development of GC compressive strength for various types of curing conditions (e.g. ambient, steam and oven curing). The investigation included grade 40, 50, and 60 MPa GC mixtures (5.8, 7.0, 8.7 ksi, respectively). The specimens were cured at 60°C (140°F) for 24 hours using hot air oven and steam curing. Out of these three curing conditions, heat curing (hot air or oven curing) gave the best results.

2.1.4. Long-Term Performance and Fire Resistance. Hardjito et al. (2004) conducted a series of experiments on the creep and shrinkage strains in GC. The creep specimens were loaded up to 40% of the compressive strength to produce a sustained stress. The creep strain was 1000 m after 12 weeks. The drying shrinkage strains were extremely small. The creep factor (ratio of creep strain-to-elastic strain) were 30 % after 6 weeks. It was found that beyond this time, the increase in creep factor was minimal. The resistance of GC to sulfate attack was examined also, the test specimens were soaked in a 5% sodium sulfate (Na_2SO_4) solution for 12 weeks, and there were no significant changes in the compressive strength, the mass, and the length of test specimens.

Aldred and Day (2012) studied the fire resistance of GC under a test duration of 2 hours. They stated that GC performed considerably better than would be expected for CC when exposed to equivalent cellulose fire.

2.1.5. Cost and CO2 Emission. Mathew et al. (2013) found that GC can be prepared at comparable cost with CC, if the provided transportation system for the raw materials was well established. Regarding the energy consumption, it was found that the embodied energy of fly ash-based GC, was 40 % less than CC. Regarding the cost of alkaline activators contribution to the total cost of GC, the proportions were 34% and 21% for sodium hydroxide and sodium silicate, respectively.

McLellan et al. (2011) stated that using geopolymer in large scale, likely lead to lower costs due to large orders of reagents. Even though, there is a significant potential for geopolymers to be cost effective and environmentally beneficial compared to traditional concrete. Depending on the binder-source location, the energy source and the mode of transportation, GC can financially and environmentally be efficient. The study indicated a potential reduction of 44% to 64% in CO_2 emissions while the financial costs were ranged from 7% lower to 39% higher compared to CC.

2.2. STRUCTURAL BEHAVIOR

The structural behavior study of geopolymer concrete initiated in Curtin University, Perth, Australia, by Sumajouw et al. (2005), it was found that the flexural load-carrying capacity increased with the tension reinforcement ratio, and the experimental values exceeded the AS-3600 predicted values.

Jeyasehar et al. (2013) compared between reinforced geopolymer and conventional concrete beams and observed higher cracking and higher ultimate flexural load, higher

mid-span deflection as well as smaller crack width for the reinforced geopolymer concrete beams.

2.2.1. Shear Behavior. There are few studies carried out to evaluate the shear behavior of reinforced geopolymer concrete until now. For beams under flexural loading, the mechanism of shear failure and corresponding shear strength of GC beams was found to be identical to that of CC beams of similar design. The shear force transfer was similar in both beam types as well as the shear strength. It was concluded that GC flexural members can be designed using existing ACI 318 methods developed for CC, and that was applied for both the service and ultimate limit states of flexural and shear capacities (Yost et al. 2013). However, Mourougane et al. (2012), observed higher shear strength of GC beams than the corresponding CC beams, in the range of 4.5–23%. Nevertheless, Mourougane et al. (2012) found that ACI 318-08 gave good prediction of the shear strength of GC beams, with an average test-to-prediction ratio of 0.96, whereas AS 3600 underestimate the shear strength of GC by giving an average test-to-prediction ratio of 1.4. Through a similar investigation on a series of shear-critical geopolymer concrete beams with different longitudinal and transverse reinforcement ratios, (Chang 2009) concluded that the provisions and the method of calculating shear strength in AS 3600 and ACI 318-08 for CC beams could be safely used to predict the shear strength for the GC beams. The average test-to-prediction ratio that obtained from experiment and AS 3600 was 1.70 and the one from experiment and ACI 318-08 was 2.55. In addition, more accurate prediction of the shear strength was achieved by using Vecchio's Disturbed Stress Field Model (DFSM) for GC beams and gave test-to-prediction ratio of 1.08 (Vecchio 2000).

To study the cross-section shape on the shear strength of GC, Madheswaran et al. (2014), studied the shear behavior of GC T-beams, since thin-webbed T-beams are generally susceptible to shear. The study included web shear-reinforced and web shear-unreinforced beams, also the shear span-to-depth ratio (a/d) varied from 1.9 to 2.5 in this study. It was observed that the performance of the beams was influenced by their compressive strength and stirrup spacing. The results indicate that the performance of GC is similar to that of CC beams and the ultimate loads are in the same order. In addition, the ACI 318-08 design of shear reinforcement was conservative and it can be safely used to design GC beams in shear, with an average test-to-prediction ratio of 1.4 for web shear-reinforced beams. The total deformations in the post-cracking, pre-yield stage include both flexural and shear deformations. The loss of shear rigidity far exceeds that of flexural rigidity and needs to be suitably accounted for when designing thin webbed T-GC beams.

The addition and effect of steel fibers on shear strength of GC beams were studied by NG (2011). It was found that adding steel fibers to GC resulted into the delay of the shear cracking, and more but finer cracks were formed in the specimens, and consequently, cracking load and ultimate strength of the steel fiber GC beams (SFGC) were increased. In addition, use of straight steel fibers resulted in a higher crack-width compared to the hooked-end steel fibers, that because the straight fibers were in a smaller diameter. To hold a comparison between the experimental and the theoretical values of SFGC, a combination of sectional shear model (Foster 2010) and strut-and-tie model were constructed. It was found that the experimental results comply with the analytical results with average test-to-model ratio for the shear capacity of 1.03, and it was concluded that SFGC beams were

more ductile and the failure of the beams were well-controlled. The SFGC beams exhibited higher deformation capacities than that of CC at failure.

NG and Foster (2011) explored the shear behavior of lightweight steel fiber GC-hollow beams (LWSFGC), reinforced with aramid fiber reinforced polymer (AFRP) bars and (AFRP) strengthened core. The shear strength of end hooked SFGC beams (without strengthened core) was 139% higher than plain GC beams. For the strengthened core beams, the shear strength of end hooked SFGC beams was 150% higher than plain GC beams. The flexural stiffness was found to be increased in SFGC; that was due to the increase of the tensile strength and the bridging effect of fibers at crack, leading to more ductile behavior.

2.2.2. Reinforcement-Concrete Bond Strength. Since GC is different in terms of chemical reaction and matrix formation compared to CC, the bond properties of GC have to be clearly understood before consider it to be suitable to replace CC structures. Sofi et al. (2007) studied the effect of different fly ash-to-slag ratio on the bond strength of the steel reinforcement and compared the test results with the available standards. It was found that the average test results-to-the prediction ratio were 1.8 for ACI 318-02 and 1.7 for AS 3600, and 2.5 for EC 2.

Using results from lap-spliced beams, Chang (2009) also found that provisions such as AS 3600 and ACI 318-08 were conservative to predict the bond strength of the lap-spliced of GC beams. The variables in that study were the splice length, the cover/bar diameter ratio, and the concrete strength. It was found that the average test-to-prediction ratio was 1.25, when the experimental values compared with ACI 408R-03 values. Chang et al. (2009) also added that the best analytical model for the lap-spliced bond strength

beams, where the model proposed by Canbay and Frosch (2005) that gave the closest match to the experimental bond strength of the GC beams, with average test-to-prediction ratio of 1.17.

2.2.3. Fracture Mode of Steel Fiber Geopolymer Concrete. In terms of fiber bridging effect on steel fiber GC, NG (2011) studied the effect of steel fiber orientation angle on the fracture mode and bond of the steel fiber in GC. Two modes of discrete steel fiber pullout tests were made. Mode I was a pull-out test of two halves of GC specimens that had various fiber inclination angles. It was found that 66% of the specimens had pulled out fibers and 34% had fractured fibers, in addition it was concluded that the snubbing effect dominates the behavior at high angle orientations of the fibers. However, Mode II was a push-off test of two L-shaped GC specimens. It was found that 21% of the specimens had a pullout fibers and 79% had fractured fibers, and it was observed that the fibers effect was minimal when the inclination angle was negative, whether fractured or polled out, that because the sharp and acute angle at the separation plane increases the snubbing of the fibers before they engaged effectively to pick up the load.

2.2.4. Effect of Shear Span-to-Depth Ratio on Shear Behavior. The shear span, a, is defined as the distance between the support reaction and a point of concentrated loading. The shear span-to-depth ratio, a/d, is a significant parameter for beams without transverse (shear) reinforcement. Generally, when a/d ratio decreases, the shear strength increases, and the increase in shear strength is significant in case of a/d less than about 2.5 to 3.0 (Hawkins et al. 2005), because, a considerable amount of shear may transmit directly to the support by a compression strut or what called arch action. Relatively, for members

that considered deep beams or at the end of beams, the design is controlled by strut-and-tie model rather than sectional design approach.

The shear span-to-depth ratio, also, relates the ultimate flexural and shear strengths in simply-supported beams with point loads, where

$$\frac{M_u}{V_u d} = \frac{a}{d}$$

In addition, the a/d ratio characterizes the slenderness of the member (see the fig. below). For simply-supported rectangular-cross section beams that have no transverse reinforcement, the mode of failure is classified as follows (ASCE-ACI committee 426 (1973) and Hawkins et al. 2005):

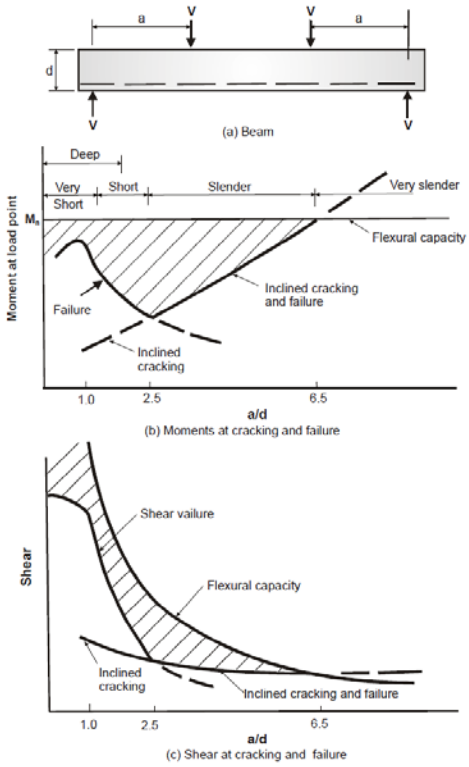

Fig. 2.1. Effect of a/d on shear strength of beams without stirrups (McGregor et al. 1997)

1) a/d less than 1.0; very short beams, most of the shear force is transferred to support by arch action, the possible mode of failure are:
   a. *Anchorage failure* of the tension steel at the end of the tie.
   b. *Bearing Failure* by concrete crushing at the support.
   c. *Flexural failure* due to tension steel yielding or crushing of the compressive zone.
   d. *Compression strut failure* by crushing of the web along the line of the crack.
2) a/d between 1.0 and 2.5; short beams, the diagonal crack pattern may produce the following possible failures:
   a. *Shear-tension failure* by the propagation of the diagonal crack along the tension steel causing bond loss and splitting between the concrete and the longitudinal bars.
   b. *Shear-compression failure* by the propagation of the diagonal crack toward the top of the beam, resulting into the crushing of the compression zone.
3) a/d between 2.5 and 6.0; slender beams, the possible failure is *diagonal-tension failure*, where the diagonal cracks (flexure and flexure-shear cracks) propagate up toward the loading plate, and down toward the support, causing the yielding of the tension steel.
4) a/d more than 6; very slender beams, where the beam fail in flexure, likely, before the formation of the inclined cracking.

The shear span-to-depth ratio, a/d, defines the slenderness of the beams. The deep beams are members loaded on one face and supported on the opposite face so that a compression concrete strut develop between the load point and the support, resisted by a steel tie in the tension zone of the member. These beams usually designed by strut-and-tie modeling or taking into account the nonlinear distribution of strain (ACI 318-8). In the strut-and-tie model, there are two regions; one is the B-region where the plane sections

remain plane after the flexural loading; and the other region is the D-region or discontinuity in the stress distribution occurs at an abrupt change in geometry or loading. The clause 10.7.1 (b) in ACI 318 define the deep beam as the region with concentrated loads within twice the member depth form the face of the support. The commentary of Appendix A (clause RA.1) in ACI 318, states that if the beam has two overlapped or convergent D-regions, the member could be designed as a single D-region. The maximum a/d ratio in this case would be 2.0. Thus the minimum angle between the compression strut and the tie is about 25°; however, the Australian Standards (AS 3600) limit that angle to 30° or higher, and the European standard (Eurocode 2 (2005)) –Design of concrete structures defines the strut inclination angle as θ from the tie axis, where $\cot\theta_{min}$ equals to 2.5 and $\cot\theta_{max}$ equals to 1.0.

If a/d is more than 2.0; that means there is a B-region between the D-regions within the shear zone. Hence, if both regions have the same reinforcement and geometry; the design will be governed by the smaller shear capacity of the B-region and the beam could be designed based on sectional shear in the ACI 318.

AASHTO - the Bridge Design Specifications- (AASHTO LRFD 2014) states that; for deep members in which the distance between the centers of the applied load and the supporting reactions is less than about twice the member thickness; the strut-and-tie model is considered.

The Canadian code (CSA 2004) consider the member as a deep beam if the distance from the point of zero shear to the face of the support is less than two times the effective depth; or if the load that causes more than 50% of the shear at the support is located in a

shear zone less than two time the effective depth from the face of the support to the load point (kong 2006).

The Japanese code (JSCE 2007) defines deep beams based on the span-to-depth ratio, *l/h*, where *l* is the beam span, and *h* is the height of the beam. The member is considered a deep beam if:

1) *l/h* is less than 2.0 for simply supported beams.
2) *l/h* is less than 2.5 for continuous beams with two spans.
3) *l/h* is less than 3.0 for continuous beams with three or more spans.

PAPER

I. SHEAR BEHAVIOR OF REINFORCED ALKALI-ACTIVATED FLY ASH-BASED GEOPOLYMER CONCRETE

Noor S. Yacob[a], and Mohamed A. ElGawady[b]

[a] Civil, Architectural and Environmental Engineering, Missouri University of Science and Technology.

[b]Associate Professor and Benavides Faculty Scholar; Civil, Architectural and Environmental Engineering, Missouri University of Science and Technology, corresponding author.

HIGHLIGHTS

- The findings provide the optimum mixture component and curing system.
- The shear behavior of reinforced geopolymer concrete beams was investigated.
- The shear deformation vs. the shear stress was investigated.

ABSTRACT

Geopolymer concrete is a revolutionary synthetic material that combines sustainability and high engineering properties, and it is relatively cost-effective compared to portland cement-based concrete, its traditional competitor. Limited research on the structural performance of versus the microstructural and material properties has been conducted until now, thus this research focuses on the shear behavior of fly ash-based geopolymer concrete. The main three factors that affect the shear strength are dowel action, shear reinforcement ratio, and shear span-to-effective depth ratio. The experimental program consists of six beams: one Conventional Concrete beam and five Geopolymer Concrete beams. Two beams had no stirrups and different flexural reinforcement ratio, two beams had different shear reinforcement ratio (i.e., different stirrup spacing, s) and one

beam had higher shear span-to-effective depth ratio (i.e., a/d). All the beams failed in shear except two beams; one had higher a/d ratio and one had smaller s. These beams failed in flexural-shear mode. All the GC beams showed high shear strength.

Keywords

Reinforced concrete; Sustainable structures; Geopolymer concrete, Fly ash; Shear strength; Shear deformation; Structural behavior

1. Introduction

Ordinary Portland Cement (OPC) production including mining, crushing, and grinding limestone followed by calcination process of calcium carbonate (limestone) into calcium oxide (lime) under very high temperatures resulting in a massive carbon dioxide footprint on the atmosphere [1]. In addition, OPC is not the ideal binder for construction in aggressive environments [2]. Over the past decades, numerous studies have been done to partially or completely replace the use of OPC in concrete by several alternative binders including industrial by-products to improve concrete durability and sustainability. Yet, none have been widely accepted as an alternative binder. For example, it is common practice in the U.S. to replace about 30% of OPC by fly ash (FA) which is a mineral substance of formative particles, mainly alumino-silicate-based ceramic spheres with minimal amounts of iron-rich spheres [3]. Juenger et al. [2], presented a review of potential alternatives to OPC including calcium sulphoaluminate cements, magnesium cements, the magnesium phosphate system, blast furnace slag, and fly ash.

In the 1970s, Davidovits developed a new class of concrete material called geopolymer concrete where 100% of OPC was replaced with aluminosilicate-rich material such as fly ash, blast furnace slag, rice husk, metakaolin, and red mud [4]. This new

material is activated using alkaline solution. The chemical reaction which is called geopolymerization takes place between the aluminosilicate and alkaline solution resulting in an inorganic amorphous three-dimensional polymeric chain and ring structure consisting of Si-O-Al-O bonds [5-8].

The schematic formation of geopolymer material can be described by Equation 1 [9]. As shown in the equation, the geopolymerization is quite different from the common hydration process which takes place in conventional concrete.

$$n(Si_2O_5, Al_2O_2) + 2nSiO_2 + 4nH_2O + (Na^+, K^+) \rightarrow n(OH)_3 - Si - O - \underset{\underset{(OH)_2}{|}}{Al^-} - O - Si - (OH)_3 \quad (1a)$$

$$n(OH)_3 - Si - O - \underset{\underset{(OH)_2}{|}}{Al^-} - O - \underset{\underset{(OH)_3}{|}}{Si} \rightarrow (Na^+, K^+) - (-Si - O - \underset{\underset{O}{|}}{Al^-} - O - \underset{\underset{O}{|}}{Si} - O -)_{\underset{O}{|}}n + 4nH_2O \quad (1b)$$

Fly ash is the more common aluminasilicate material used for geopolymer concrete manufacturing. Based on ASTM C618 [10] specification, the chemical requirements of fly ash in terms of SiO_2+Al_2O_3+Fe_2O_3 content must be greater than 70% for Class F fly ash (low calcium content), and 50% for class C fly ash (higher calcium content) to be considered a rich alumino-silicate material. Class F is more successful in producing geopolymer concrete as it has higher content of silicate and hence more reactivity. The higher calcium content in class C leads to opportunity for chlorides to react with calcium to form calcium chlorides ($CaCl_2$) [11]. To ensure a high level of stability needed for good durability, the Sulfur Trioxide (SO_3) should be less than 1% [12].

The chemistry of the alkali liquid plays an essential role on properties of geopolymer concrete. Several researchers investigated using sodium hydroxide with sodium silicate, and potassium hydroxide with potassium silicate as alkaline liquids [13]. It was found that, the combination of sodium silicate and sodium hydroxide resulted in the higher compressive strength compare to mixtures prepared using potassium hydroxide with potassium silicate. Moreover, sodium silicate-to-sodium hydroxide ratio of 2.5 resulted in the highest compressive strengths. Sodium hydroxide molarity ranging from 8 M to 14 M resulted in acceptable strengths [14 and 15].

Geopolymer concretes based on class F fly ash take longer time to set and develop strength in ambient temperatures [16]; however, heat curing at temperatures ranging from 60°-90°C can accelerate strength development [17]. This temperature range can be reduced by using high calcium fly ash class C [18] as the higher calcium content produces Calcium-Silicate-Hydrate gel, C–S–H, which can be cured at ambient temperatures [12].

2. Shear behavior in geopolymer reinforced concrete

While there have been numerous studies on shear strength of conventional concrete, research on shear strength of geopolymer concrete is scarce. Recently, reinforced fly ash-based geopolymer concrete beams were tested under four-point bending [19]. It was found that the Australian Standards AS-3500 and ACI 318-08 [20 and 21] were able to conservatively predict the shear strength of investigated beams. It was also showed a good correlation between the test results and a finite element model incorporating the disturbed stress field method.

Sarker et al. [22] studied the fracture behavior of fly ash-based geopolymer concrete and found that the fracture energy increased with increasing the concrete compressive

strength The measured fracture energy for geopolymer concrete were higher than those measured by Bazant and Giraudon [23] for conventional concrete; however, Sarker et al. [22] found that failure modes of GC specimens were more brittle than those of CC specimens. The difference in behavior was attributed to the higher bond and tensile strength of GC. The dense interfacial transition zone of GC resulted into higher critical stress intensity and more brittle type of failure with smoother fracture plane as compared to CC specimens.

3. Research significance

Geopolymer concrete is studied exhaustively on the material side; most of the literature analyzed the microstructure and the chemical composition of geopolymer concrete. So far limited studies investigated the structural behavior of geopolymer concrete due to the difficulty associated in transferring from small scale to large scale in terms of material handling and curing regime. Therefore, this research represents one of the pioneer studies to investigate the shear strength of geopolymer concrete beams which should help design engineers to implement geopolymer concrete in their future structural designs. The shear strengths of the investigated beams were compared to those obtained using the shear provisions in ACI 318-08 [21], AASHTO [24], CSA [25], EC 2 [26] , AS-3600 [20], and JSCE [27] specifications.

4. Experimental program

4.1. Specimen details

The research presented in this manuscript includes testing five GC beams and one CC. Each beam had a span of 2,438 mm (96 in.). All the beams had rectangular cross sections of 203 mm (8 in.) in width and 305 mm (12 in.) in height with variable shear reinforcement in the form of U-shaped stirrups (Fig. 1 and 2). All beams were designed

according to ACI 318 [21] to fail in shear with calculated shear strengths ranged from 27% to 75% of their flexural strengths.

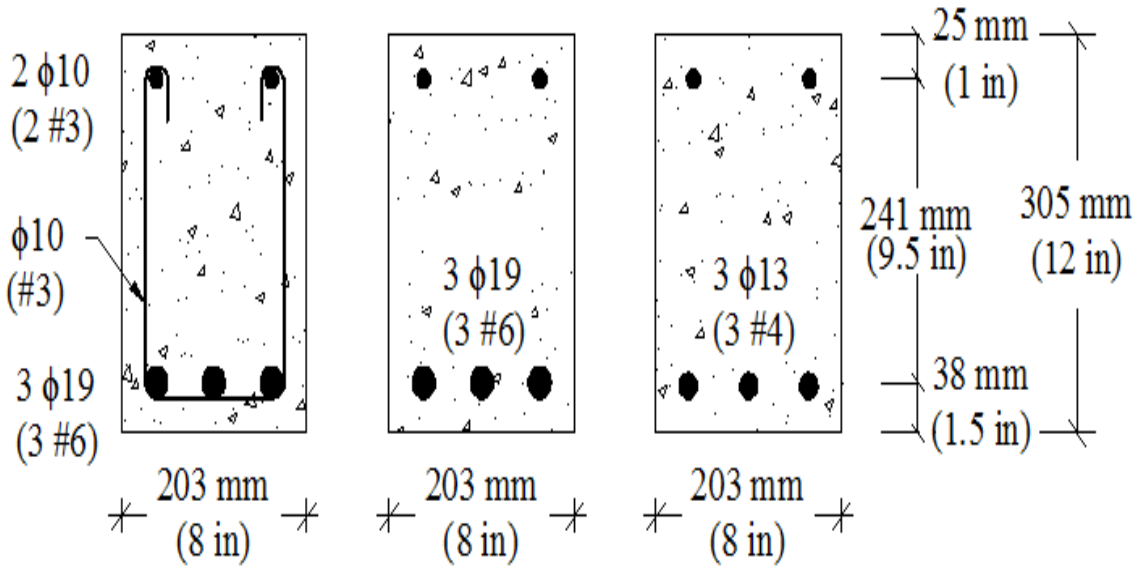

Fig. 1. Different cross-sections of the beams

The nomenclature of the test specimens consists of four parts (Table 1). The first part is a letter presenting the type of the concrete: G for geopolymer and C for conventional, the second part is a letter representing the existence and spacing between shear reinforcement in the shear span region: N for no shear reinforcement, L for large spacing of 254mm (10 in.), and S for small spacing of 191 mm (7.5 in.). The third part is a number representing the diameter of the longitudinal reinforcement bar in the US custom units: 6 for 19 mm diameter and 4 for 13 mm diameter bars. The last part is a number representing the value of a/d.

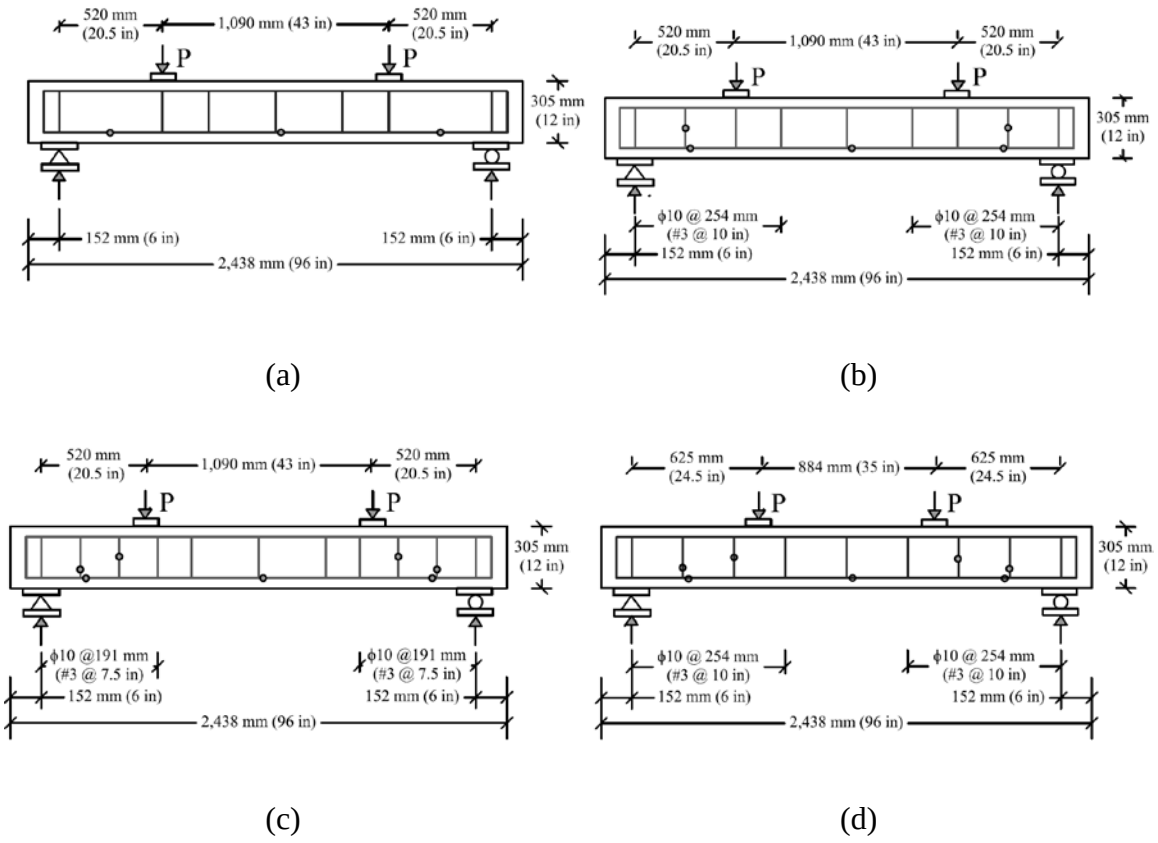

Fig. 2. Load pattern and location of strain gages of the test beams
(a) Without stirrups within the shear region (a/d = 2),
(b) Stirrups at large spacing (a/d= 2),
(c) Stirrups at small spacing (a/d = 2), and
(d) Stirrups at large spacing (a/d = 2.4)
- Location of strain gauge

Two beams, namely GN6-2 and GN4-2, had no shear reinforcement within the shear span region while the remaining beams had 10 mm (No. 3) diameter rebar as shear reinforcement at spacing of either 191 mm (7.5 in.) or 254 mm (10 in.) (Table 1 and Fig. 1 and 2). Five beams had shear span-to-effective depth ratio (a/d) of 2.0. The sixth specimen, GL6-2.4, had a/d of 2.4. Five beams had longitudinal flexural reinforcement ratio (ρ_w) of

1.57% corresponding to the balance reinforcement ratio (see Table 1). The sixth beam, GN4-2, had ρ_w of 0.71% corresponding to the balance reinforcement ratio (see Table 1).

Table 1. Test matrix

Section	Flexural reinforcing	Top hangers	ρ_w	ρ_b	Stirrups	a/d
GN6-2	3 ϕ19 (3#6)	2 ϕ10 (2#3)	0.0157*	0.0249	_	2.0
GN4-2	3 ϕ13 (3#4)	2 ϕ10 (2#3)	0.00706**	0.0239	_	2.0
GL6-2	3 ϕ19 (3#4)	2 ϕ10 (2#3)	0.0157*	0.0290	ϕ10@254 mm (#3@10 in.)	2.0
GL6-2.4	3 ϕ19 (3#4)	2 ϕ10 (2#3)	0.0157*	0.0272	ϕ10@254 mm (#3@10 in.)	2.4
GS6-2	3 ϕ19 (3#4)	2 ϕ10 (2#3)	0.0157*	0.0272	ϕ10@191mm (#3@7.5 in.)	2.0
CL6-2	3 ϕ19 (3#4)	2 ϕ10 (2#3)	0.0157*	0.0281	ϕ10@254 mm (#3@10 in.)	2.0

*ρ_{min} = 0.00246 ** ρ_{min}= 0.00297

4.2. Materials

4.2.1. Aggregates

The coarse aggregate was crushed dolomite to minimize the water and chemical liquids absorption; hence, to keep the aggregate moisture condition close as much as

possible in saturated-surface-dry (SSD) condition. The nominal maximum aggregate size was 13 mm (1/2 in.). The fine aggregate was natural river sand taken from Missouri River.

4.2.2. Fly ash

Two different types of class F fly ash were used during the course of this study. The chemical composition and physical properties of the two types of fly ash is shown in Tables 2 and 3, respectively. As shown in the table, the fly ash had low calcium oxide content of 7.49% and 8.30% for Type 1 and 2 respectively. The fly ash Type 1 was unsuccessful.

4.2.3. Alkali liquid and HRWR

The alkali activators were a combination of sodium hydroxide (NaOH) solution and sodium silicate (Na_2O_3Si) solution. The NaOH solids were commercial grade with purity more than 99% in pellets form. The sodium silicate solution was type D™ with silicate acid and sodium salt of 44.1%, water content of 55.9%, and specific gravity of 1.53 g/cm^3 at 20°C (95.5 lb/ft^3 at 68°F). The NaOH solution was prepared 24 hours prior to the mixing day, to let the solution reach the room temperature.

Different trial mixtures had NaOH molarity of 8M, 14M and 16M, two types of sodium silicate solutions (i.e., N® and D™), different rest time period of zero and 5 hours (i.e. the time between casting and curing), and mixing process (i.e. A: for mixing fly ash with dry ingredients, and B: for mixing fly ash directly with the liquid activators) (see Table 4 and Fig. 3).

Based on these trial mixtures, trial mix number 6 had the best combination of strength and slump values. Hence, this mixture was used in the remaining of this research. For mixture number 6, the required NaOH molarity was obtained by adding 404 grams of

sodium hydroxide pellets to 596 grams of distilled water to create one kilogram of NaOH solution of 14M.

Table 2. Chemical composition of fly ash

FA type	Type 1	Type 2
Source (state)	TN	TX
SiO_2[1]	48.28	59.27
Al_2O_3[2]	20.14	22.09
Fe_2O_3[3]	15.22	5.15
Sum of [1'2'3]	83.63	86.51
CaO	7.49	8.30
MgO	1.07	1.62
SO_3	2.41	0.44
Na_2O	0.92	0.15
K_2O	-	1.08
LOI	1.14	0.30

Table 3. Physical properties of fly ash

	Type 1	Type 2
Retained on #325 Sieve, %	14.1	29.22
Specific Gravity	2.45	2.25
Moisture Content, %	0.12	0.03

Table 4. Trial mixtures

Mix no.	Rest time (hours)	Sodium hydroxide (molarity)	Sodium silicate (type)	Extra-added water	HRWR	Mixing process (type)	Fly ash (type)
1	-----	8M	N®	Yes	Yes	A	1
2	5	8M	N®	Yes	Yes	A	2
3	5	14M	N®	Yes	Yes	A	2
4	0	16M	D™	Yes	Yes	A	2
5	0	14M	D™	Yes	Yes	A	2
6	0	14M	D™	Yes	Yes	B	2
7	0	14M	N®	Yes	No	B	2
8	0	14M	N®	No	Yes	B	2

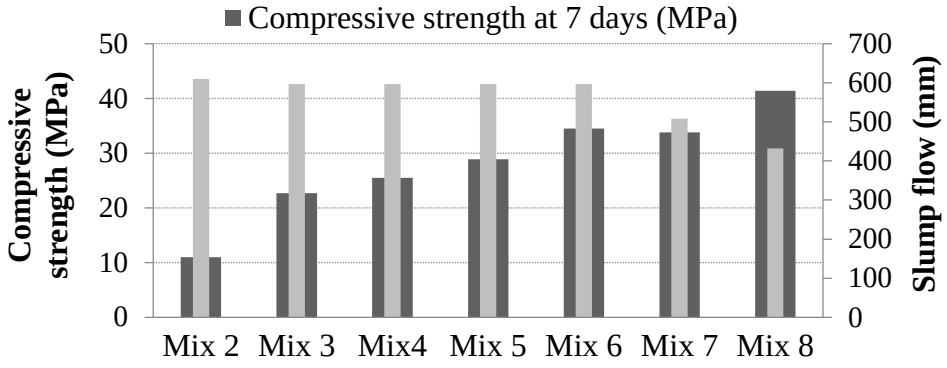

Fig. 3. Compressive strength and slump flow of trial mixtures

A high-range water-reducer (HRWR), Glenium-7500, admixture was added to improve the workability. The chemicals were mixed together on the mixing day in plastic pails, and the HRWR along with the extra-added water were mixed in a separate pail.

4.2.4. Steel reinforcement

The used steel reinforcement bars were ASTM A615 [28] Grade 60. The steel bars properties were determined according to the ASTM A370 [29] and the results are presented in Table 5.

Table 5. Longitudinal and transverse reinforcement properties

Bar No.	Yield Strength, MPa (ksi)	Ultimate Strength, MPa (ksi)	Modulus of Elasticity, MPa (ksi)
ϕ 10 (#3)	490 (71)	714 (104)	196,500 (28,500)
ϕ 13 (#4)	464 (67)	717 (104)	191,000 (27,700)
ϕ 19 (#6)	561(81)	797 (116)	194,000 (28,200)

4.3. Mixture proportions

Table 6 indicates the mixture proportions used during this research. Similar mixture was used by several researchers in the literature (e.g. [19 and 30]). The average slump flow measured per ASTM C1611 [31] was 605 mm (23.8 in.) in diameter (Fig. 4). The flowability of the mix is attributed to the spherical shape of the fly ash particles in combination with the lubricating effect of sodium silicate solution. No signs of segregation were observed, which complies with the mixing requirements of GC [12].

A gravity mixer of 0.17 m^3 (6 ft^3) was used for the mixtures. The fly ash was mixed with the chemical liquids first for one minute to ensure full contiguity, and then the fine and coarse aggregate was added along with the extra-added water and the HRWR. The

mixing continued for five more minutes. The liquids-to-cementitious material ratio was 0.43 by weight.

Table 6. Mixture proportions

Material	Kg/m^3	lb/ft^3
Coarse Aggregate	1194	74.4
Fine Aggregate	643	40.1
Class F Fly Ash	406	25.3
Sodium Hydroxide Solution	41	2.6
Sodium Silicate Solution	103	6.4
HRWR	6.1	0.4
Extra Added Water	25.6	1.6

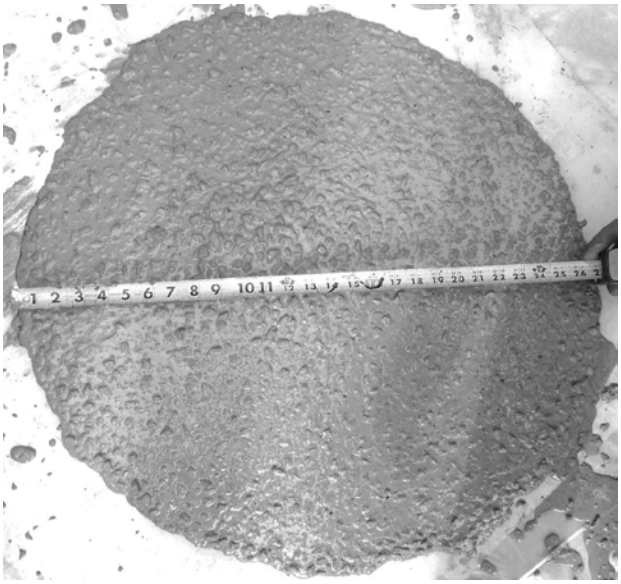

Fig. 4. Slump flow of GC

4.4. Curing time

Curing is crucial for geopolymer concrete. To determine the curing time that yields an acceptable strength, a set of geopolymer concrete cylinders were prepared using the mixture shown in Table 6 and the procedure described in the previous section. The cylinders were cured in the oven at 65°C (150°F) for different periods of time ranging from 1 to 28 hours. Fig. 5 shows the effects of curing period on the strength of the cylinders, each value represents the average of three test cylinders. As shown, the concrete gained most of its strength within the first four hours of curing when the strength reached to 20 MPa (3000 psi). Beyond that the strength gain rate is relatively smaller and the concrete reached about 35 MPa (5000 psi) at 24 hours of curing. Hence, during the beams testing a curing of 24 hours at 65°C (150°F) was used.

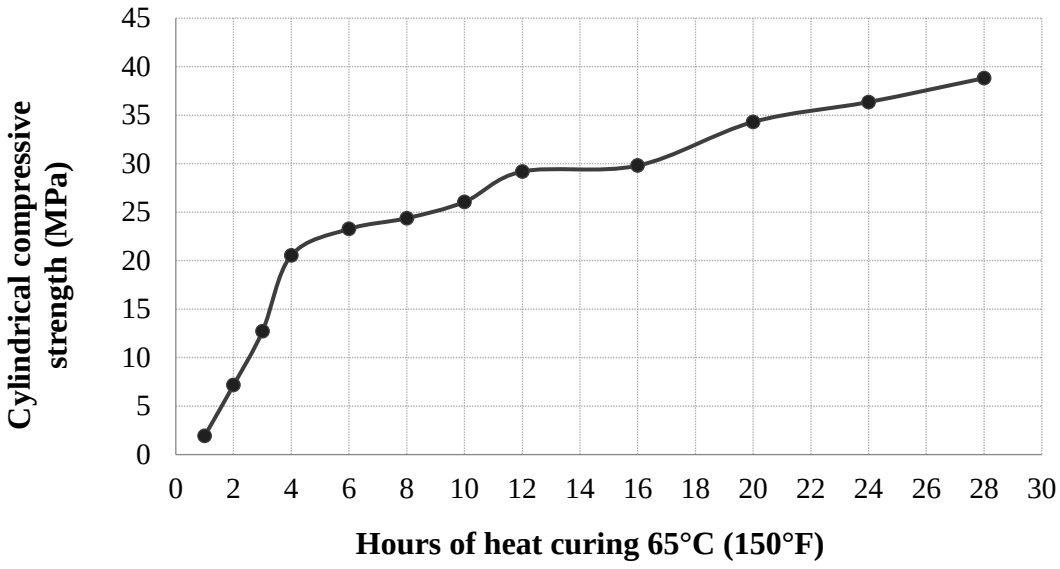

Fig. 5. Heat curing effect

4.5. Fabrication and curing of test specimens

The geopolymer concrete mixture described earlier in this manuscript was prepared and poured into a steel formwork (Fig. 6). Once the fresh concrete poured into the formwork, it was placed into environmental chamber at 65°C (150°F) for 24 hours. Three thermocouple wires Type T [Copper/Constantan; reads from -270 to 370°C (-454 to 700°F)] were installed on three different locations along the beam centerline to monitor the temperature along the length of each beam (Fig. 6). A quality control assurance companion 100 x 200 mm (4 x 8 in.) cylinders confronting to ASTM C39 [32] were cast and cured in the same regime and tested in the same test day of each beam. Table 7 presents the fresh and hardened concrete properties per the appropriate ASTM standards. The unit weight of the fresh mix was 1,623 kg/m^3 (100 lb/ft^3) per ASTM C138 [33].

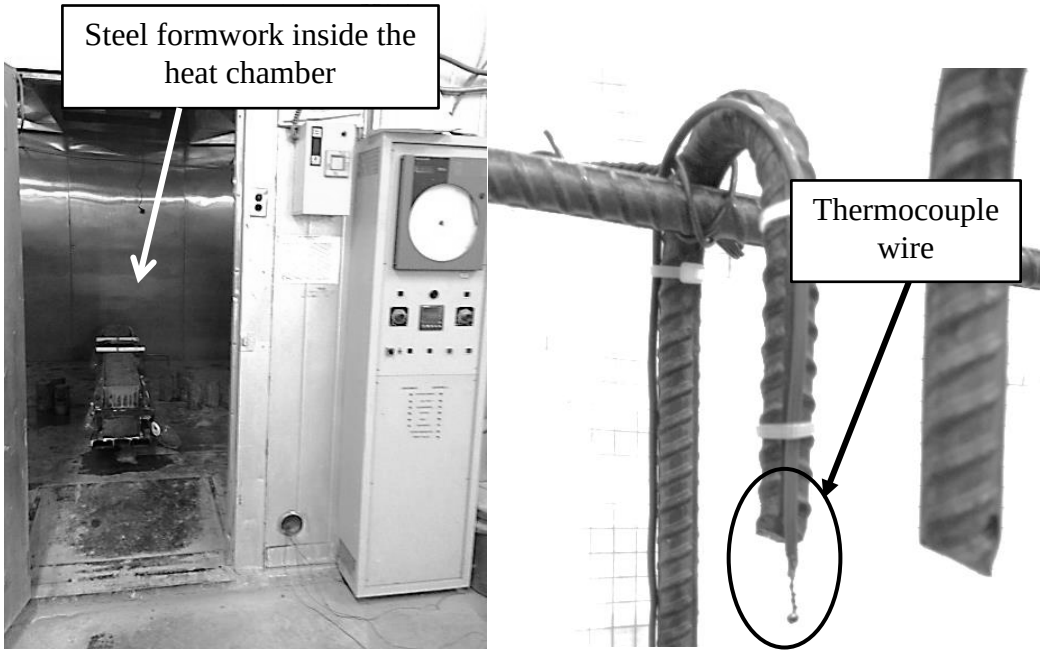

Fig. 6. Heat-curing (left) and thermocouple wire (right)

The beams were removed outside the environmental chamber after curing; then, demolded and kept uncovered in the lab ambient temperature until the test day (Fig. 7). The average age of the specimens at the test day was 60 days.

Fig. 7. Test specimens after curing

Table 7. Fresh and hardened concrete properties

Beam ID	Slump Flow[a], mm (in.)	Compressive Strength, f'c, MPa (ksi)	Modulus of Elasticity, MPa (ksi)	Splitting Tensile Strength, MPa (ksi)	Air-void content[c] (%)
GN6-2	609 (24)	37.2 (5.4)	29,647 (4,300)	2.63 (381)	3.26
GN4-2	660 (26)	26.9 (4.0)	24,132 (3,500)	1.77 (257)	4.16
GL6-2	584 (23)	43.4 (6.3)	29,992 (4,350)	2.14 (311)	2.05
GL6-2.4	584 (23)	43.4 (6.3)	30,682 (4,450)	2.34 (340)	------
GS6-2	584 (23)	41.2 (6.0)	28,096 (4,075)	2.32 (337)	------
CL6-2	114[b] (4.5)	43.4 (6.3)	41,369 (4,600)	2.94 (427)	3.39

[a] Slump flow pre ASTM C1611 (ASTM 2009);
[b] Slump per ASTM C143 (ASTM 2010);
[c] Air-void content per ASTM C457 (ASTM 2012).

The air-content in hardened GC and CC was measured per ASTM C457 [34] using an air-void analyzer (RapidAir-457). After the structural testing, disk specimens were cored from three GC beams that had different compressive strengths as well as from the CC beam. The results are illustrated in Table 7, and images of GL6-2 are shown in Fig. 8.

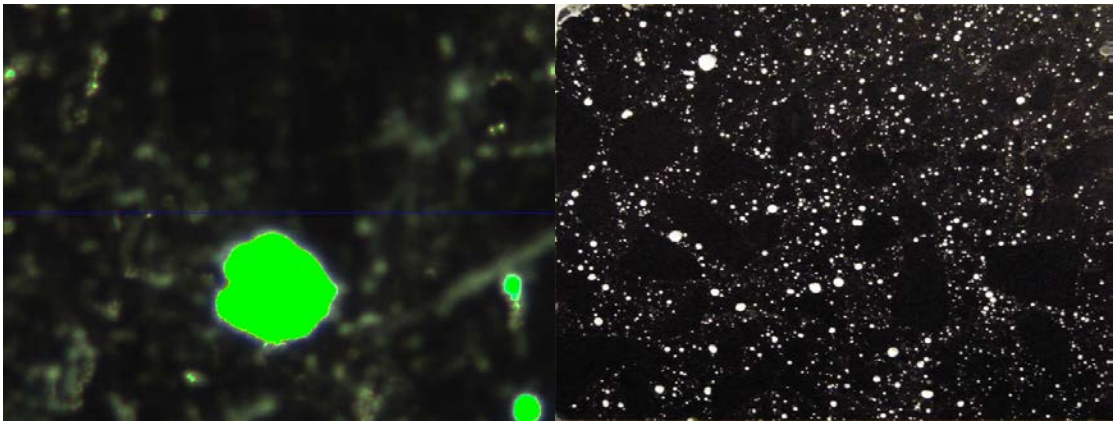

Fig. 8. Air-void images of GL6-2. Analyzed image (left) and test sample image (right)

As shown in the table, for the same compressive strength, the geopolymer concrete had lower air-void ratio compared to conventional concrete. Furthermore, for the geopolymer concrete, the higher the strength is the lower air-void content.

4.6. Test setup and procedure

The beam was simply supported using a roller on one side and pin on the other side. The load was applied by two 490-kN (110-kip), servo-hydraulic actuators, to a strong W-shaped beam which applied the load at two loading points to the beam creating a four-point

load configuration (Fig. 2). The load was applied in a displacement-control at a loading rate of 0.5 mm/min (0.02 in./min) until failure occurred.

Linear variable differential transformers (LVDT) were fixed at mid-span on both sides of each beam and under the applied load points. Four LVDTs were also installed on each side of the beam within *d* distance from the support (Fig. 9). Electrical resistance strain gauges were also mounted on the longitudinal reinforcement at mid-span and mid-shear span to measure the axial strains at these critical locations during the test. Strain gauges were also installed on both legs of the stirrups (Fig. 2).

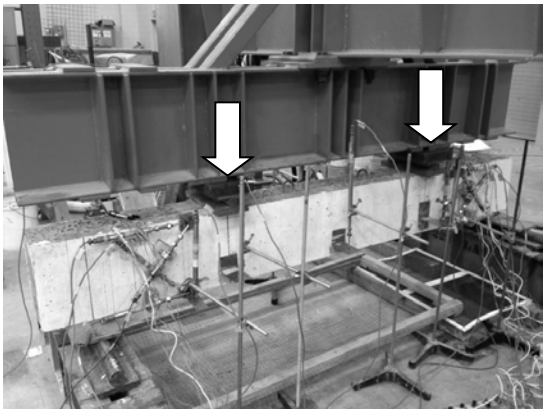

Fig. 9. Test setup and measurement system

5. Experimental results

5.1. Cracking and failure modes

All beams failed in shear except beam GL6-2 that failed in torsion. The beam was misplaced in the testing rig resulting in out of plane eccentricity. Table 8 summarizes the modes of failure, shear force at failure (V_{test}), average shear stress at failure ($V_{test}/b_w d$),

and ratio of the average shear stress to square root of the compressive strength ($v_{test}/\sqrt{f'_c}$) for beams without shear reinforcement.

Generally, cracks formation and propoagation in geopolymer beams were similar to these typically observed in conventional reinforced concrete beams. Flexural cracks initiated in the maximum moment region followed by minor flexural cracks formed in the shear span region between the support and the loading point. By increasing the applied displacement, most of the flexural cracks propagated upward toward the compression zone of the beam and shear cracks appeared near the supports and propagated upward toward the loading plate. The formed crackes started to widen with increasing the applied displacement. In addition, horizontal shear-tension cracks observed near the supports in the case of the GN6-2, GL6-2.4, and GN4-2 (Fig. 10).

For the beams that failed in flexure-shear, diagonal shear cracks developed during the test; then, crushing of the concrete at midspan between the loading plates in the compression zone occurred acompained by a significant deflection. For the beams that had shear reinforcement, all the stirrups where yielded (see Fig. 11)

Table 8. Test results summary

Beam ID	Failure mode[a]	$V_{test}, kN(kips)$	$v_{test} = \frac{V_{test}}{b_w d}, MPa\ (ksi)$	$\frac{v_{test}}{\sqrt{f'c}}$
GN6-2	S	209 (47.0)	3.95 (573)	0.65
GN4-2	S	128 (28.8)	2.39 (347)	0.46
GL6-2	T-S	186 (41.7)	3.51 (509)	------
GL6-2.4	F-S	203 (45.6)	3.83 (555)	------
GS6-2	F-S	237 (53.3)	4.48 (650)	------
CL6-2	S	214 (48.0)	4.04 (586)	------

[a] S: Shear; S-T: Torsion-shear; F-S: Flexure–Shear.

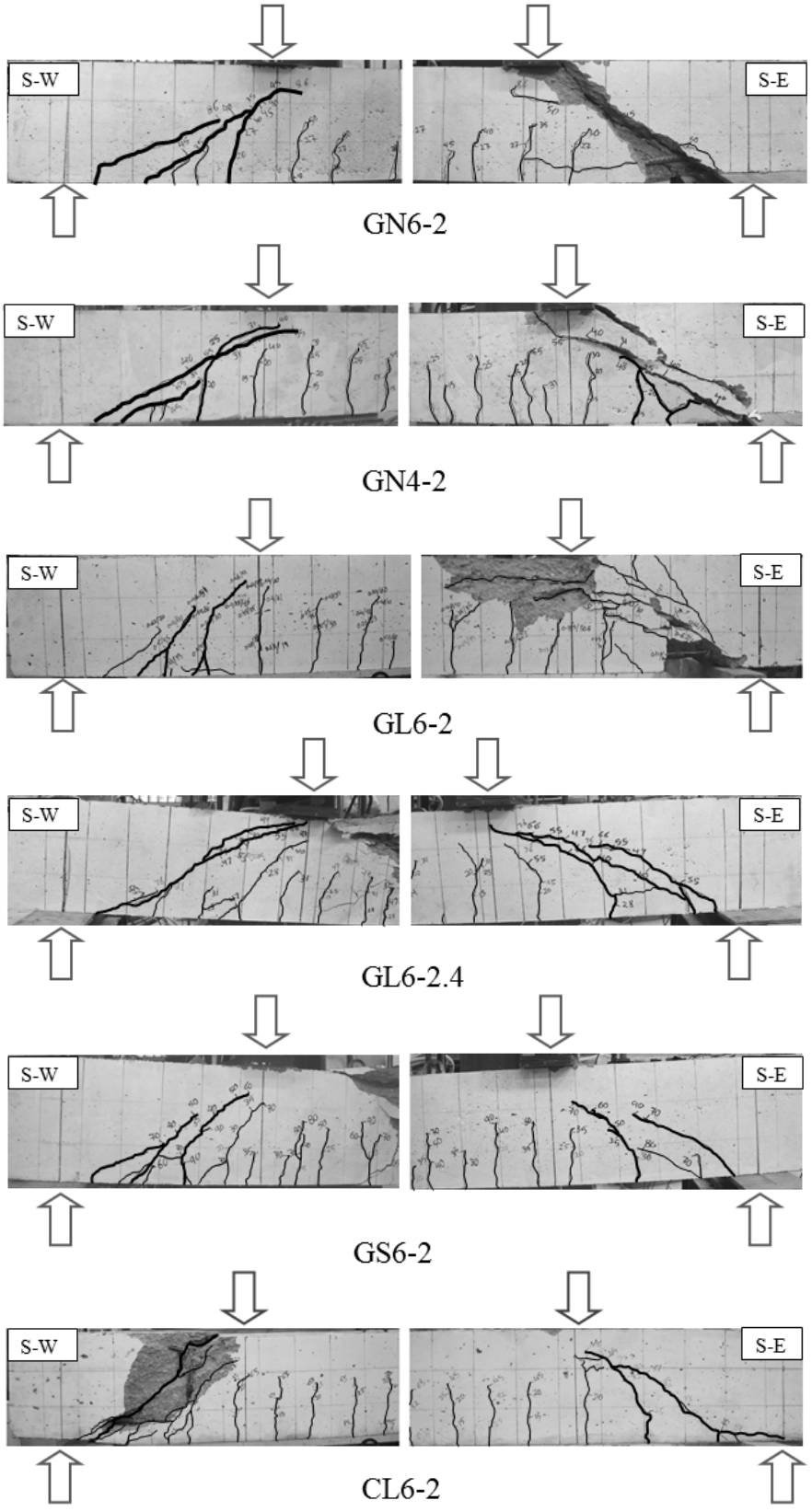

Fig. 10. Crack pattern and mode of failure

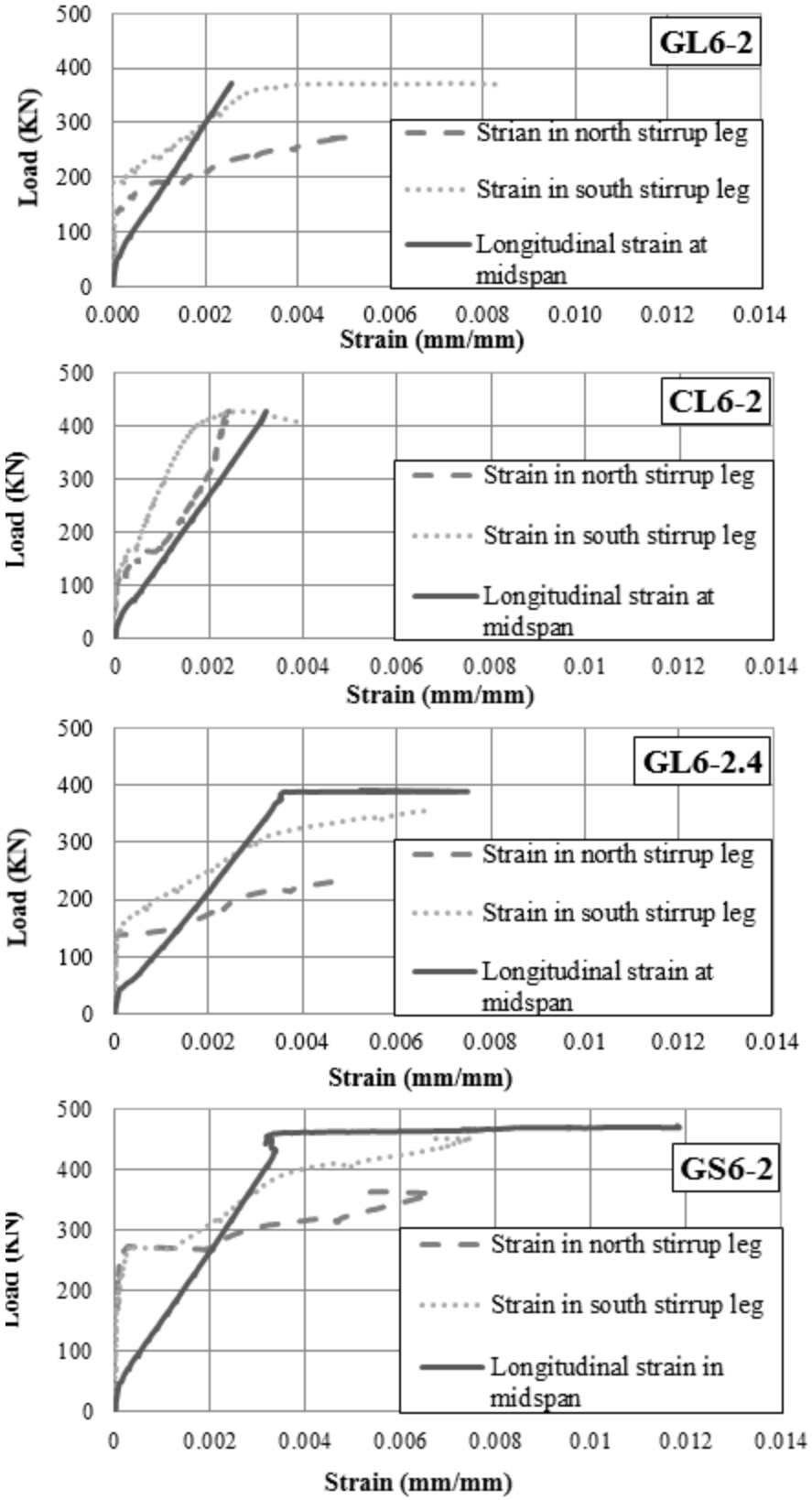

Fig. 11. Strain gauge readings

Crack progression in GL6-2 and CL6-2 were identical except for the diagonal crack that developed on the top of GL6-2 due to combined torsion and shear (Fig. 12). A spall of concrete (i.e. compression-shear failure) was observed on both beams near the loading plate (Fig. 10).

Fig. 12. Failure mode of GL6-2

For beams without shear reinforcement, The crack progression and morphology was identical for GN6-2 and GN4-2. The failure was brittle, and the diagonal compression sturt in both beams spalled out in a huge chunk of concrete at time of ultimate failure (Fig. 10).

For the beams without shear reinforcing, failure occurred when the inclined flexure-shear crack penetrated to the compression zone of the beam near the loading plate before

yielding of the longitudinal reinforcement, as observed in Fig. 10. For the beams with shear reinforcing, failure occurred when the stirrups crossing the critical flexure-shear crack reached yield.

From Table 8, it can be seen that the maximum shear stress in GL6-2 was the lowest among the beams with shear reinforcement because of the combined torsion and shear failure that occurred during the test, as seen in Fig. 12. That combined failure also reduced the shear strength compared to CL6-2 that had the same compressive strength. Furthermore, due to the shear-flexure failure in GL6-2.4 and GS6-2, it can be inferred that the shear strength of these beams was higher than shown in Table 8. By investigating GN6-2, with the presence of ϕ19 (#6) longitudinal reinforcement, the shear strength was enhanced by the direct dowel action that contributed significantly to the shear capacity. The dowel action had also an indirect contribution to control the diagonal shear crack width that consequently affected the aggregate interlock (friction) between the aggregate and the paste. Commonly, the aggregate interlock refers to the interaction between the rough surfaces of the shear crack, and it relatively influences the shear capacity. From Fig. 12, it can be seen that the crack split the aggregate and created a smooth surface, which means that the paste is strong enough to fully transfer the ultimate critical shear stress to the aggregate sections and there was a good bond between the paste and the aggregate.

The last column in Table 8 shows the factor relative to equation (11-3) in ACI-318 [21], rewritten in terms of average shear stress for normal-weight concrete and shown as:

$$v_c = 0.17\sqrt{f'_c}\ (MPa) \qquad or \qquad v_c = 2\sqrt{f'_c}\ (psi) \tag{2}$$

The ratio of experimental shear stress to square root of compressive strength for the beams GN6-2 and GN4-2 exceeded the ACI value of 0.17 by 280% and 170 %, respectively, which indicates the conservativeness of ACI to evaluate the concrete shear capacity, implying that the code equation is too conservative to be applied for geopolymer concrete.

For GL6-2, the stirrups were yielded at 61% of the peak-shear load while the longitudinal steel at midspan was not yielded, whereas the stirrups and the longitudinal steel at midspan was yielded at 77% of the peak-shear load for CL6-2. For the beams without shear reinforcement, the longitudinal reinforcement at midsapn was yielded at 83% and 58% of the peak-shear load for GN6-2 and GN4-2, respectively. For GL6-2.4, the first stirrup was yielded at 48% of the peak load before the longitudinal steel at midspan that yielded at 68% of the peak load. For GS6-2, the first stirrup was yielded at 62% of the peak load before the longitudinal steel at midspan that yielded at 76% of the peak load. The second stirrups were not yielded for either beam. This behavior showed that the failure in these beams was a combination of shear and flexure.

Fig. 13 shows the load-deflection response of the tested beams. The curves show the behavior of the specimens up to the peak load varied with the displacement in flexure midspan. It can be seen that the stiffness of GL6-2 and CL6-2 beams were identical. For the beams without shear reinforcement, there was a difference in stiffness between the two beams, thus, GN4-2 tend to fall in a more ductile behavior than GN6-2 due to the lower reinforcement ratio (ρ_w) and lesser stiffness. The GL6-2.4 beam reached the peak load of GL6-2, and then proceeded to a ductile type of failure until the crushing of concrete in the top fiber between the two loading plates. This behavior was owed to the increase in a/d

value from 2.0 to 2.4. The GS6-2 beam failed in a same mode of GL6-2.4 (flexure-shear), but it had a higher peak load than GL6-2 because of the higher shear reinforcement ratio (less spacing between the stirrups) that increased the shear capacity of the beam.

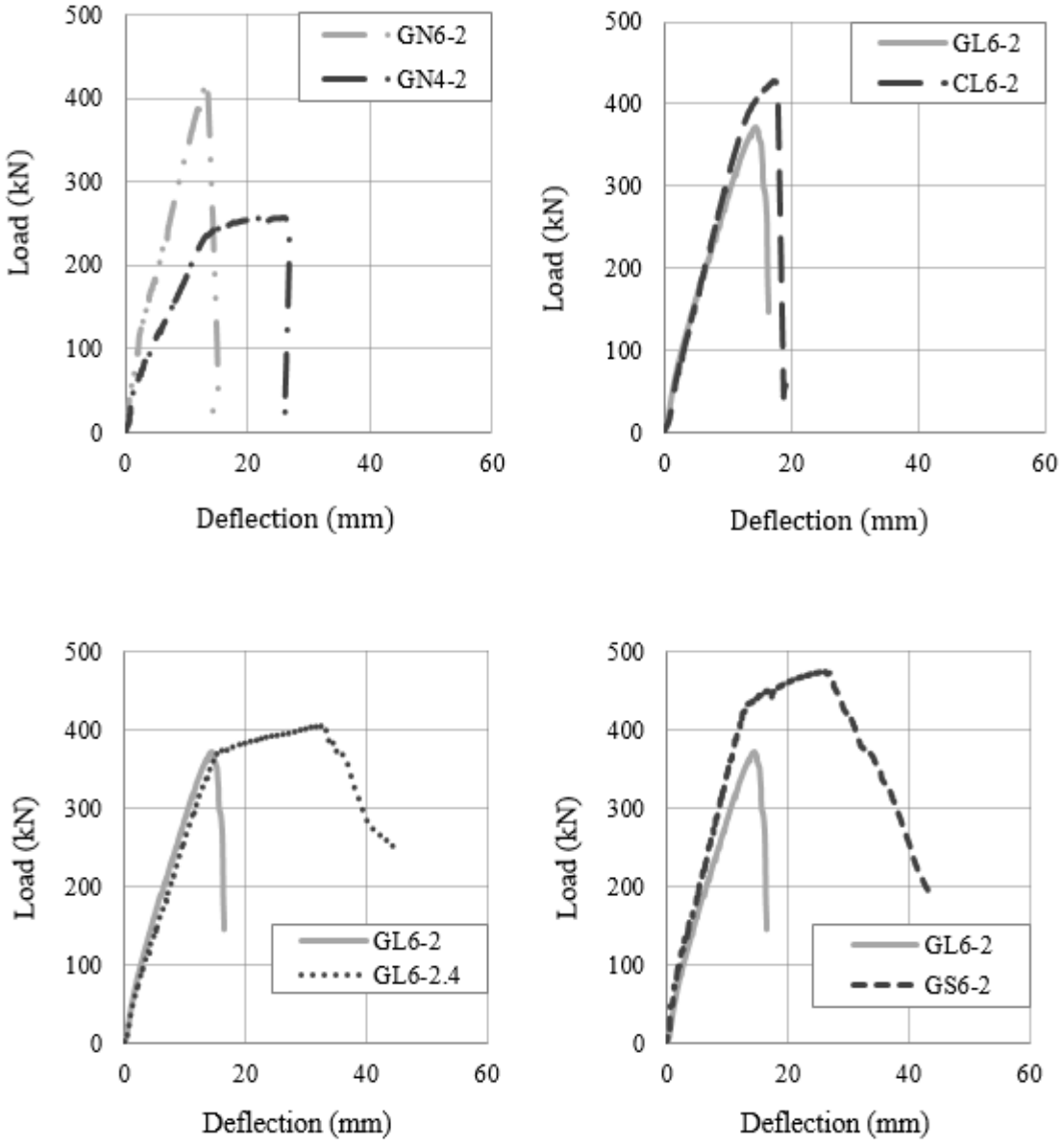

Fig. 13. Load deflections of the test beam

The toughness of a material is the ability to absorb energy within the plastic region without rupture, and it represents the balance between the strength and the ductility. For the behavior shown in Fig. 13, the toughness is calculated as the area under the curve. The toughness factor, T.F., was taken equal to the toughness of the modified beam-to-the toughness of the reference beam. For the GC and CC beams, T.F. was equal to 1.3, means the CC beam was more ductile that the GC beam. However, for the beams without shear reinforcement, T.F. was 1.1, since the failure of both GN4-2 and GN6-2 was brittle and had no ductility. Conversely, T.F. was larger for the beams that failed in flexure-shear (i.e. GL6-2.4 and GS6-2) of 3.8 and 4.2 respectively, due to the ductile failure of these beams compared to the reference GL6-2.

5.2. Evaluation of shear deformations and strains of the test specimens

The shear deformations at the ends of the test specimens were calculated using the attached diagonal LVDTs (Fig. 9). Fig. 14 shows the end of a beam having a length of *l* and height of *h* before and after deformation; both lengths were taken equal to d. The beam is subjected to flexural and shear deformations, where the shear deformation can be calculated as follows:

$$y_{S1} = \frac{\sqrt{(\Delta_{s2})^2 - l^2} - \sqrt{(\Delta_{s1})^2 - l^2}}{2} \tag{3a}$$

Assuming the flexural deformation at the top and bottom of the beam are identical, i.e., $y_f = y_{f1} = y_{f2}$; hence, the total deformation, y_t, along line BC can be obtained as follows:

$$y_t = y_s + y_f = \frac{\sqrt{(\Delta_{sd2})^2 - (l + x_2)^2} - \sqrt{(\Delta_{sd1})^2 - (l + x_1)^2}}{2} \tag{3b}$$

Where Δ_{sd1} and Δ_{sd2} are the measured diagonal deformations due to the combined flexure and shear actions, x_1 and x_2 are the measured horizontal displacements at the top and bottom fibers of the beam respectively.

The flexural deformation (y_f) is attributed to the rotation of the horizontal cords of the top and bottom fibers of the beam (Fig. 13) and can be evaluated as follows:

$$\theta_{sd} = \frac{x_1 - x_2}{h} \tag{4a}$$

$$\delta_f = \alpha \, l \, \theta_{sd} \tag{4b}$$

Where,

α is a factor that describes the distance from the top of the section to the centroid of the sectional curvature distribution.

The center of rotation is located at the centroid of the beam segment in case of no flexural effect. Therefore, α is assumed to vary from 0.5 for rectangular distribution to 0.67 for the triangular distribution. In this case (rectangular distribution), α was taken equal to 0.5, assuming that the center of rotation is located at the mid-height of the AD element, and θ_{sd} is the angle of rotation [35 and 36].

The values of $\Delta_{sd1}, \Delta_{sd2}$, x_1 and x_2 were obtained from readings of the LVDTs shown in Fig. 9. The shear stresses vs. shear drifts of the test specimens are shown in Fig. 15, where the shear drift ratio is defined as the shear deformation normalized by the shear span (a).

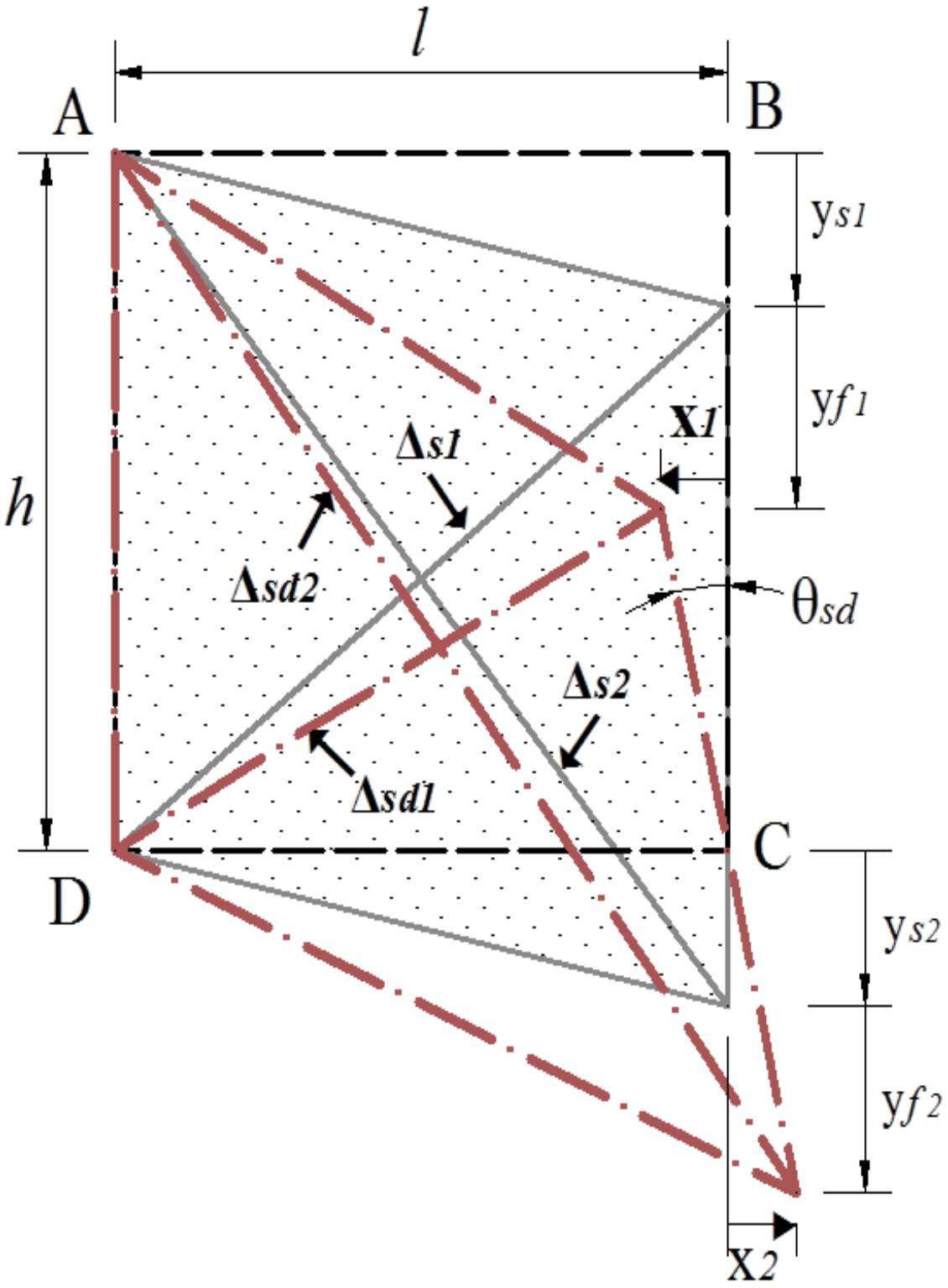

Fig. 14. Deformed configuration reproduced after Jirawattanasomkul et al. [36]

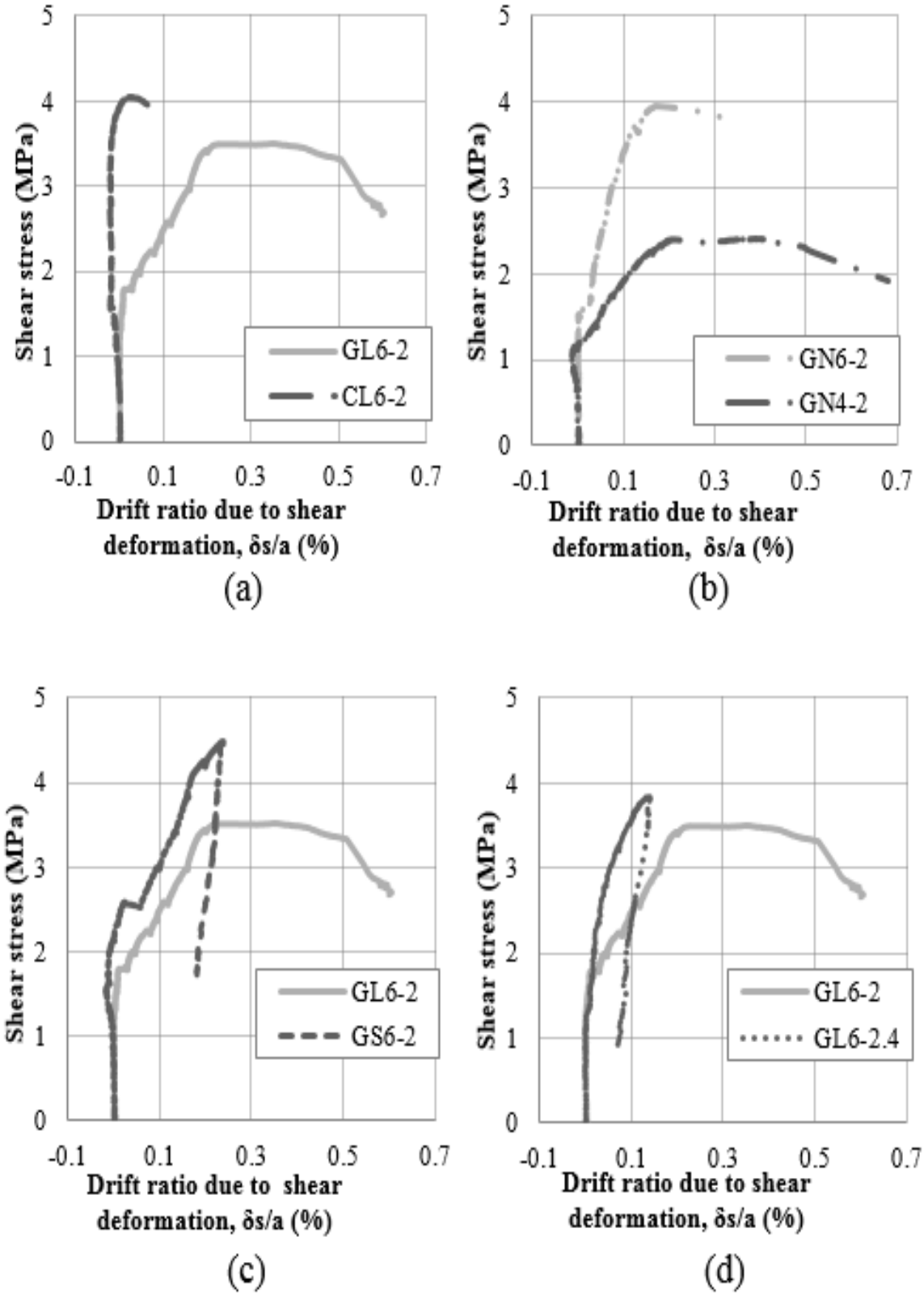

Fig. 15. Shear stress versus drift ratio due to shear deformation

The average shear strain across the diagonal cracking within shear region can be also calculated as follows [37]:

$$\gamma = \frac{\delta_2 - \delta_1}{\sqrt{h^2 + l^2}} \quad (5)$$

Where δ_1 and δ_2 are the displacements in the direction of the compression strut and across the shear crack, respectively. Both were measured using the diagonal LVDTs (Fig. 9). Fig.16 shows the relationship between the shear stress and the average calculated shear strain. It also shows the initiation of the shear diagonal crack (I.D.C.).

As shown in Fig. 15 and 16, all beams displayed the same shear stiffness until the I.D.C. Beyond first cracking, the different test parameters affected the performance of the beams. As shown in Fig. 15(a) and 16(a), both geopolymer and convectional concrete beams displayed the same shear stiffness. However, the accidental torsion demand on the geopolymer beam, GL6-2, significantly increased the shear deformation compared to CL6-2 beam. In addition; the shear deformation calculation of CL6-2 stopped at 0.1% due to the loss of LVDT readings. Furthermore, increasing the flexural rebar ratio decreased the shear deformations due to the dowel action (Fig. 15(b), 16(b)); however, it increases the shear stresses. Decreasing the spacing between stirrups increased the shear stiffness (Fig. 15(c) and 16(c)). However, since the mode of failure of specimen GS6-2 was flexural-shear, the shear deformation beyond the beak load significantly decreased since the beam deformation was mainly resulted from flexural deformations. Similarly, beam GL6-2.4 displayed smaller shear deformation beyond the peak load (Fig. 15(d)).

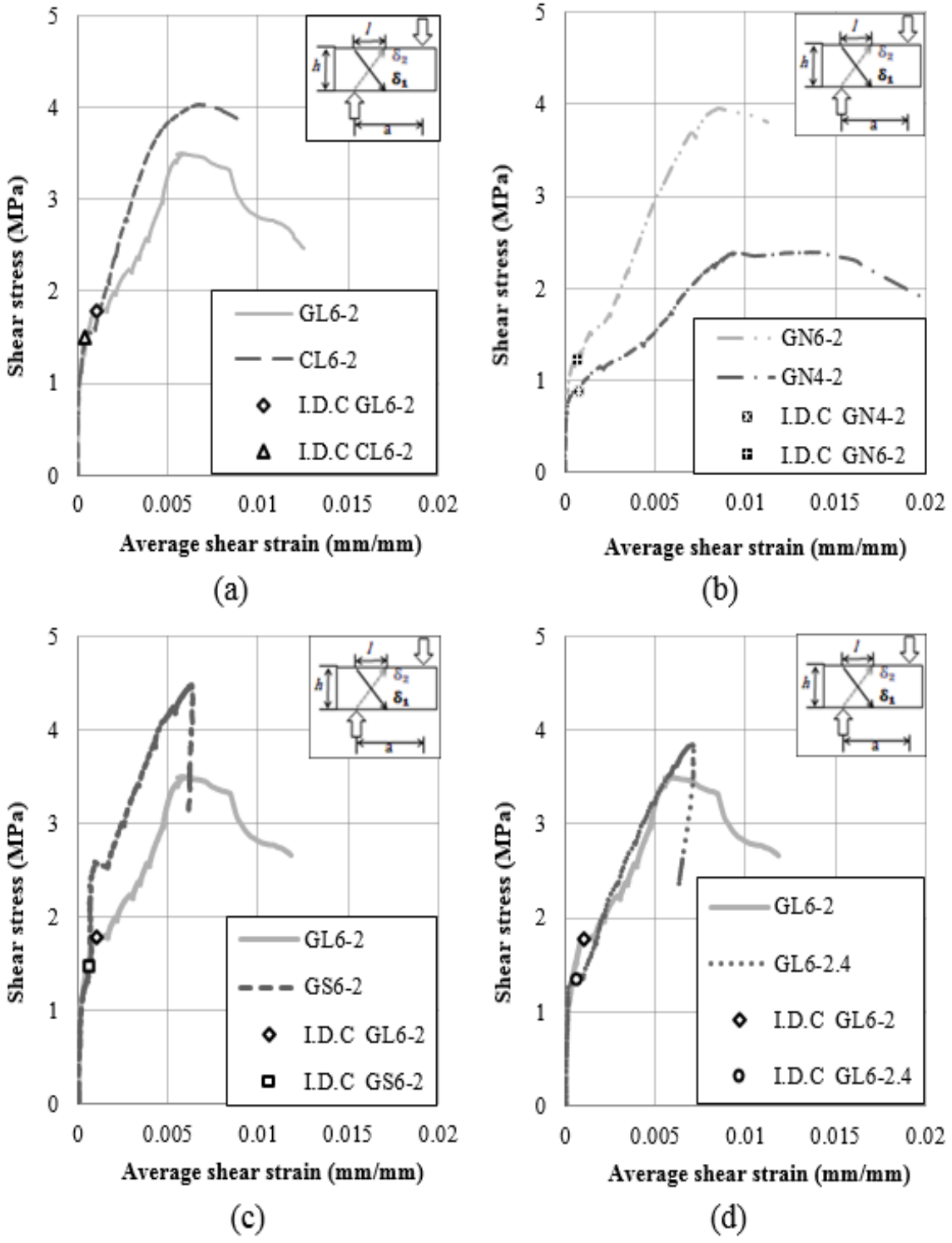

Fig. 16. Average principle shear strain versus the shear stress

5.3. Comparison of test results with shear provisions of different international standards

The measured material properties and the dimensions of each beam were used to calculate the shear strengths of each beam using the shear provisions of the AASHTO [24], ACI 318-08 [21], AS-3600 [20], CSA [25], Eurocode 2 [26], and JSCE [27]. All the standards resisting and load factors were set to one for ultimate moments and shear force calculations. The calculated shear strengths were compared to those measured during the experimental work.

The codes evaluate the shear strength of reinforced concrete using different approaches and theories. Generally, these provisions count the contributions of many sources such as the shear friction (aggregate interlock), direct tension across diagonal cracks, dowel action of flexural bars, arch action, and stirrups. As many factors influence the contributions of each of these mechanisms, typically empirical or semi-empirical expressions were developed for shear strength of concrete beams. For example, some codes use the flexural effective depth (d) to evaluate the shear strength (e.g., ACI 318, AS-3600, JSCE 2007, and EC-2), others (e.g., AASHTO and CSA) use the effective shear depth (d_v) taken as the perpendicular distance to the neutral axis between the resultants of the tensile and compressive forces due to flexure. Some codes use the cubic root of the characteristic concrete compressive strength (e.g., AS-3600, EC-2, and JSCE 2007); others (e.g., AASHTO, ACI 318, CSA) use the square root of the characteristic concrete compressive strength. Some standards (e.g. ACI 318, and JSCE 2007) use a constant angle model (i.e., 45 degrees) while others (e.g., AASHTO and CSA) use compression field theory, i.e., variable truss angle model to evaluate the shear strength provided by stirrups (V_s).

Table 9 presents the ratio of experimental to code-predicted capacity (V_{test}/V_{code}) for the selected design standards for all the beams. As shown in the table, all the ratios are greater than one, indicating that all investigated standards are conservatively predicting the shear strength of the GC and CC beams. For beams without shear reinforcement, the ratio of V_{test}/V_{code} varies from 2.07 to 4.34 with the JSCE having the closest prediction and AASHTO having the farthest prediction of shear strength.

Table 9. Ratios of analytical to experimental shear strengths of the test specimens

Section	AASHTO	ACI	AS-3600	CSA	EC-2	JSCE	Response 2000
GN6-2	4.34	3.59	3.18	4.05	2.99	2.34	2.98
GN4-2	3.09	2.72	2.81	2.89	2.64	2.07	2.45
Average	3.72	3.15	2.99	3.47	2.81	2.20	2.75
COV (%)	23.79	19.49	8.73	23.63	8.78	8.65	13.80
GL6-2	1.36	1.40	1.14	1.32	1.17	1.24	1.06
GL6-2.4	1.29	1.54	1.09	1.25	1.13	1.36	1.16
GS6-2	1.70	1.81	1.43	1.65	1.47	1.60	1.13
Average	1.45	1.58	1.22	1.41	1.25	1.40	1.11
COV (%)	15.12	13.16	15.04	15.18	14.78	13.09	4.59
CL6-2	1.70	1.61	1.41	1.64	1.45	1.43	1.22

COV= coefficient of variation.

Generally, all codes were better predictor of the shear strength of the shear-reinforced beams because of the higher predictability of the shear strength portion provided by the stirrups. For GC beams with shear reinforcement, the ratio of V_{test}/V_{code} ranges from 1.09 to 1.81. The AS-3600, EC-2, and JSCE had higher fidelity in predicting the shear strength of the tested specimens with average values of V_{test}/V_{code} of 1.22, 1.25, and 1.40, respectively. The ACI-318, AASHTO, and CSA relatively overestimated the shear strength of the tested specimens with with average values of V_{test}/V_{code} of 1.58, 1.45, and 1.41, respectively.

In addition to the international shear provisions of shear presented in Table 9, the software Response 2000 [38] were used to investigate the shear strength of the tested beams based on the modified compression field theory (MCFT). From the average of the ratio of the beams without shear reinforcement, Response 2000 was the closest prediction except of JSCE code. For the beams that had shear reinforcement, Response 2000 was the most agreement with the experimental even for the CC beam. From these results, it was inferred that Response 2000 was less conservative to predict the shear strength of the geopolymer concrete beams.

5.4. Comparison of reinforcement strains from experiment and AASHTO LRFD

The simplified method in lieu of the general procedure -that involves more accurate calculations to determine the shear resistance of concrete- uses specified values of β and θ terms both in AASHTO LRFD and CSA, where β is the factor reflecting the effect of longitudinal tensile strain (ε_x) on the shear capacity of concrete, indicated by the ability of the diagonal crack to transmit the tension stress, and θ is the angle of inclined diagonal compressive stress in degrees. However, to perform more accurate but less conservative

calculation, the CSA introduced an equation for ε_x similar to the AASHTO LRFD equation. The only change is that the AASHTO LRFD equation uses ε_s (the tensile strain in the longitudinal tension reinforcement) instead of the tension longitudinal strain at mid depth (ε_x) [39]. For members containing at least the minimum amount of transverse reinforcement, ε_x will be half the sum of ε_s and ε_c where ε_s is the positive tensile strains in tension reinforcement and ε_c is the negative compressive strain in concrete that is assumed negligible. For members containing less than the minimum amount of shear reinforcement, a conservative simplification can be made by setting ε_x equal to ε_s. Based on the foregoing assumption, AASHTO equations can be rewritten (for nonprestressed members that subjected to bending and shear only and adapt the simplified assumption that $0.5 \cot \theta$ equals 1.0) as follows:

for members without shear reinforcement,

$$\varepsilon_s = \frac{\left(\frac{|M_u|}{d_v} + |V_u|\right)}{E_s A_s} \tag{6a}$$

for members with shear reinforcement,

$$\varepsilon_s = \frac{\left(\frac{|M_u|}{d_v} + |V_u|\right)}{2E_s A_s} \tag{6b}$$

The larger ε_s value will result in a higher value of θ and a lower value of β that will typically require more shear reinforcement and relatively decrease the tension force in the longitudinal reinforcement [24].

Table 10 presents the maximum experimental tensile strain in the longitudinal tension reinforcement at the middle of the shear region, obtained by the strain gauge readings and the AASHTO LRFD eq. 6. From the results, the equation overestimated the tensile longitudinal strain in all the beams. The reference GL6-2 and CL6-2 beams were the closest prediction to the equation, whereas, GN6-2, GN4-2, and GS6-2 were the furthest prediction.

Table 10. Comparison of flexure reinforcement strain from experiment and AASHTO Eq.

Section	ε_s shear midspan equation (μ strain)	ε_s shear midspan experiment (μ strain)	$\varepsilon_{s\_Eq.}/\varepsilon_{s\_Exp.}$
GN6-2	4,068	2,874	1.81
GN4-2	5,584	3,957	1.68
Average	--------	--------	1.74
COV (%)	--------	--------	5.26
GL6-2	1,805	2,938	1.09
GL6-2.4	2,246	2,889	1.43
GS6-2	230,7	2,553	1.63
Average	--------	--------	1.38
COV (%)	--------	--------	19.73
CL6-2	2,077	3,292	1.15

COV=coefficient of variation

6. Conclusions and recommendations

This paper is to evaluate the shear strength of a new sustainable material called alkali-activated fly ash-based geopolymer concrete or zero-cement concrete. The concrete mix is basically class F fly ash activated by alkali liquids (e.g., sodium hydroxide and sodium silicate). The study included five GC beams and one CC beam. Three variables were studied: the longitudinal reinforcement ratio, the transverse (shear) reinforcement ratio, and the shear span-to-effective depth ratio (a/d). The shear behavior was examined in terms of crack morphology and progression, load-deflection response, failure mechanism, strengths predicted form available design standards, longitudinal reinforcement tensile strains at failure, shear deformation, and average shear strain in concrete. Based on the results, the following conclusions are presented:

1) The crack progression was identical for beams that failed in compression-shear except the concrete crush on the top of the beam at midspan in the beams that failed in flexure-shear.
2) In terms of the load-deflection response, the GC beam showed almost the same ductility as the identical CC beam.
3) The design codes conservatively predicted the shear strength of the concrete, especially the codes implementing semi-empirical equations like AASHTO LRFD and CSA.
4) The AASHTO LRFD equation for longitudinal reinforcement tensile strains overestimated strain for GC beams without stirrups and underestimated the tensile strain for GC and CC beams with stirrups.

5) The shear deformation and the average principle strain were significant in the beams that failed in shear and torsion-shear, whereas, it was not significant in the beams that failed in flexure-shear.
6) The variation in shear span-to-depth ratio from 2.0 to 2.4, changed the the mode of failure from shear failure to flexure-shear failure.

Based on the specimen's investigation, it would appear that existing design codes for conventional concrete are equally applicable to geopolymer concrete, especially for shear strength provided by the stirrups. However, the design codes seem to underestimate the shear strength provided by the concrete. The origin of the empirical equations and formulas of design standards were based on a significant database, usually by involving two or more specimens for each variable examined to surround the high scatter associated with the shear testing; hence, this study needs to be replicated with more specimens. Furthermore, variables such as size effect, aggregate type and content, different curing systems, and durability performance under aggressive environment must also be investigated to come up with the same reliability that conventional concrete conquered by time.

Acknowledgements

The authors gratefully acknowledge Boral Technologies, San Antonio, TX for donating the second type of Fly ash class F used during this study. Appreciation is also extended to PQ Corporation, Malvern, PA for donating type D™ sodium silicate liquid. However, the conclusions and the opinions expressed in this paper are those of the authors and do not necessarily reflect the official views or policies of the aforementioned corporations.

Notation

A_s = area of non-prestressed tension reinforcement

b_w = web width

d = effective depth

E_s = steel modulus of elasticity

f'_c = spcified compressive strength of concrete

M_u = ultimate flexural capacity

V_u = ultimate shear strength

v_c = nominal shear stress provided by concrete

ε_c = compression strain in concrete

ε_s = strain in non-prestressed longitudinal tension reinforcement

ρ_b = balanced reinforcement ratio

ρ_{min} = minimum flexural reinforcement ratio

ρ_w = ratio of A_s to $b_w d$

References

[1] Struble, L. and Godfrey, J., 2004, May. How sustainable is concrete. In *International workshop on sustainable development and concrete technology* (pp. 201-211).

[2] Juenger, M.C.G., Winnefeld, F., Provis, J.L. and Ideker, J.H., 2011. Advances in alternative cementitious binders. *Cement and Concrete Research*, *41*(12), pp.1232-1243.

[3] Zahi, S. and Daud, A.R., 2011. Fly ash characterization and application in Al–based Mg alloys. *Materials & Design*, *32*(3), pp.1337-1346.

[4] Aydın, S. and Baradan, B., 2012. Mechanical and microstructural properties of heat cured alkali-activated slag mortars. *Materials & Design*, *35*, pp.374-383.

[5] Davidovits, J., 1991. Geopolymers. *Journal of thermal analysis*, *37*(8), pp.1633-1656.

[6] Davidovits, J., 1994. High-alkali cements for 21st century concretes. *Special Publication*, *144*, pp.383-398.

[7] Van Jaarsveld, J.G.S., Van Deventer, J.S.J. and Lorenzen, L., 1997. The potential use of geopolymeric materials to immobilise toxic metals: Part I. Theory and applications. *Minerals Engineering*, *10*(7), pp.659-669.

[8] Komnitsas, K. and Zaharaki, D., 2007. Geopolymerisation: A review and prospects for the minerals industry. *Minerals Engineering*, *20*(14), pp.1261-1277.

[9] Davidovits, J., 1999, June. Chemistry of geopolymeric systems, terminology. In *Geopolymer* (Vol. 99, pp. 9-40).

[10] ASTM, C., 2005. 618, Standard specification for coal fly ash and raw or calcined natural pozzolan for use in concrete. *ASTM C*, *685*.

[11] Kupwade-Patil, K. and Allouche, E.N., 2012. Examination of chloride-induced corrosion in reinforced geopolymer concretes. *Journal of Materials in Civil Engineering*, *25*(10), pp.1465-1476.

[12] Law, D.W., Adam, A.A., Molyneaux, T.K., Patnaikuni, I. and Wardhono, A., 2015. Long term durability properties of class F fly ash geopolymer concrete. *Materials and Structures*, *48*(3), pp.721-731.

[13] Palomo, A., Grutzeck, M.W. and Blanco, M.T., 1999. Alkali-activated fly ashes: a cement for the future. *Cement and concrete research*, *29*(8), pp.1323-1329.

[14] Hardjito, D., Wallah, S.E., Sumajouw, D.M. and Rangan, B.V., 2004. On the development of fly ash-based geopolymer concrete. *ACI Materials Journal-American Concrete Institute*, *101*(6), pp.467-472.

[15] Joseph, B. and Mathew, G., 2012. Influence of aggregate content on the behavior of fly ash based geopolymer concrete. *Scientia Iranica*, *19*(5), pp.1188-1194.

[16] Winnefeld, F., Leemann, A., Lucuk, M., Svoboda, P. and Neuroth, M., 2010. Assessment of phase formation in alkali activated low and high calcium fly ashes in building materials. *Construction and Building Materials*, *24*(6), pp.1086-1093.

[17] Sanni, S.H. and Khadiranaikar, D.R., 2013. Performance of Geopolymer Concrete Under Various Curing Conditions. *International Journal Of Scientific Research*, *2*(3).

[18] Guo, X., Shi, H. and Dick, W.A., 2010. Compressive strength and microstructural characteristics of class C fly ash geopolymer. *Cement and Concrete Composites*, *32*(2), pp.142-147.

[19] Chang, E.H., 2009. Shear and bond behaviour of reinforced fly ash-based geopolymer concrete beams.

[20] AS3600, A.S., 2001. Concrete structures. *AS3600-2001*. *Sydney (Australia): Standards Australia*.

[21] ACI Committee, American Concrete Institute and International Organization for Standardization, 2008. Building code requirements for structural concrete (ACI 318-08) and commentary. American Concrete Institute.

[22] Sarker, P.K., Haque, R. and Ramgolam, K.V., 2013. Fracture behaviour of heat cured fly ash based geopolymer concrete. *Materials & Design*, *44*, pp.580-586.

[23] Bažant, Z.P. and Becq-Giraudon, E., 2002. Statistical prediction of fracture parameters of concrete and implications for choice of testing standard. *Cement and Concrete Research*, *32*(4), pp.529-556.

[24] LRFD, A., 2004. AASHTO LRFD bridge design specifications.

[25] Canadian Standards Association, 2004. *Design of concrete structures*. Canadian Standard Association.

[26] No, E., 1992. 2, Design of Concrete Structures, Part 1: General Rules and Rules for buildings. *Commission of European Communities ENV*, pp.1-1.

[27] Japan Society of Civil Engineers, 2007. *Standard specification for concrete structure*. JSCE No. 15, Tokyo, 154–159.

[28] ASTM, A., 615/A 615M (2008),"Standard Specification for Deformed and Plain Carbon-Steel Bars for Concrete Reinforcement". *ASTM International*.

[29] ASTM International, 2010. *A370-10 Standard Test Methods and Definitions for Mechanical Testing of Steel Products*. ASTM International.

[30] Sumajouw, M.D.J. and Rangan, B.V., 2006. Low-calcium fly ash-based geopolymer concrete: reinforced beams and columns. *Curtin University of Technology*.

[31] ASTM, A., C1611/C1611M-09b Standard Test Method for Slump Flow of Self-Consolidating Concrete. 2009. *ASTM International West Conshohocken, PA*.

[32] ASTM, C., 2001. 39, Standard test method for compressive strength of cylindrical concrete specimens. *ASTM International*.

[33] ASTM, R., C138-Standard Test Method for Unit Weight. *Yield, and Air Content (Gravimetric) of Concrete*.

[34] ASTM. C457/C457M-12, 2012, Standard test method for microscopical determination of parameters of the air-void system in hardened concrete. *West Conshohocken, PA.*

[35] Massone, L.M. and Wallace, J.W., 2004. Load-deformation responses of slender reinforced concrete walls. *ACI Structural Journal-American Concrete Institute*, *101*(1), pp.103-113.

[36] Jirawattanasomkul, T., Dai, J.G., Zhang, D., Senda, M. and Ueda, T., 2013. Experimental study on shear behavior of reinforced-concrete members fully wrapped with large rupture-strain FRP composites. *Journal of Composites for Construction*, *18*(3), p.A4013009.

[37] Khaja, M.N. and Sherwood, E.G., 2013. Does the shear strength of reinforced concrete beams and slabs depend upon the flexural reinforcement ratio or the reinforcement strain? 1. *Canadian Journal of Civil Engineering*, *40*(11), pp.1068-1081.

[38] Bentz, E.C. and Collins, M.P., 1998. *RESPONSE-2000: Reinforced concrete sectional analysis using the modified compression field theor.*

[39] Kuchma, D.A., Hawkins, N.M., Kim, S.H., Sun, S. and KANG, S.K., 2008. Simplified shear provisions of the AASHTO LRFD Bridge Design Specifications. *PCI journal*, *53*(3), pp.53-73.

SECTION

3. SUMMARY, CONCLUSIONS AND RECOMMENDATIONS

3.1. SUMMARY OF RESEARCH WORK

The purpose of this research is to evaluate the shear strength of a new sustainable material called alkali-activated fly ash-based geopolymer concrete or zero-cement concrete. The concrete mix is basically class F fly ash activated by alkali liquids (i.e., sodium hydroxide and sodium silicate). The study included five GC beams and one CC beam. Three variables were studied: the longitudinal reinforcement ratio, the transverse (shear) reinforcement ratio, and the shear span-to-effective depth ratio (a/d). The shear behavior was examined in terms of crack morphology and progression, load-deflection response, failure mechanism, strengths predicted form available design standards, longitudinal reinforcement tensile strains at failure, shear deformation, and average shear strain in concrete. This section also presents the conclusions of the previous investigations as well as the investigation of the polymerization rate of geopolymer concrete and the air-void content in the hardened paste. Lastly, the recommendations of the author are presented in the end of this chapter for future studies.

3.2. CONCLUSIONS

The following section summarizes the conclusions from both the experimental and analytical studies of the geopolymer and conventional concrete beams.

- The optimum concentration (molarity) of the sodium hydroxide was 14M.
- No need of rest period between casting and curing.

- The best way to achieve full contiguity between the fly ash and the liquid activators was to mix them together first and then to add the other dry ingredient of the concrete.
- Lower water content yielded to lower slump flow and higher compressive strength.
- The polymerization rate was directly proportional with curing time.
- The air-void content in GC has inverse relation with its compressive strength.
- The overall impression in terms of crack morphology and progression was identical for beams that failed in shear except the concrete was crushed on the top of the beam at midspan in the beams that failed in flexure-shear.
- The design codes conservatively predicted the shear strength of both the geopolymer and the conventional concrete.
- The AASHTO LRFD equation for longitudinal reinforcement tensile strain, overestimated strain for GC beams without stirrups and underestimated the tensile strain for GC and CC beams with stirrups.
- The drift due to shear deformation and average principle shear strain were significant in the beams that failed in shear and torsion-shear failure, compared with the beams that failed in flexural-shear.
- The variation in shear span-to-depth ratio changed the mode of failure of the beams.

3.3. RECOMMENDATIONS

Based on the conclusions stated in the previous section, the following recommendations for future research were developed:

- Study the size effect of the section and the span of the beam.

- Study the aggregate size and type on shear strength of GC.
- Replicate the research with more variation in longitudinal reinforcement and shear span-to-depth ratio.
- Replicate the research with identical CC beam for each GC beam.
- Perform shear test on different cross-section shapes like I-shape girders.
- Investigate the shear strength of GC for other structural members such as columns, walls and slab panels.
- Study the cyclic load behavior of GC members.
- Investigate the durability of GC in terms of corrosion and exposure to harsh environmental conditions.

APPENDIX A

TRIAL MIXTURES OF ALKALI-ACTIVATED FLY ASH-BASED GEOPOLYMER CONCRETE

Table A.1- Mix no. 2

Mix No.	Cylinder No.	Rest period (hours)	Curing period (hours)	Curing temp. C°/F°	Age (days)	Compressive strength (psi)	Average (psi)
2-A	1	_	24 h	60/140	1 d	996	1,373
	2	_	24 h	60/140	1 d	1,572	
	3	_	24 h	60/140	1 d	1,550	
2-B	1	5 h	24 h	60/140	1 d	1,367	1,206
	2	5 h	24 h	60/140	1 d	1,177	
	3	5 h	24 h	60/140	1 d	1,075	
2-C	1	5 h	24 h	60/140	7 d	1,617	1,579
	2	5 h	24 h	60/140	7 d	1,817	
	3	5 h	24 h	60/140	7 d	1,303	
2-D	1	24 h	24 h	60/140	7 d	_	2,072
	2	24 h	24 h	60/140	7 d	2,068	
	3	24 h	24 h	60/140	7 d	2,077	

- Aggregate: 1/2 inch, crushed dolomite
- Sodium Hydroxide solution: 8M
- Sodium Silicate: type N®
- All dry materials were mixed first, then chemicals and water were added
- HRWR: Gelinum-7500
- Slump flow: 24 in

Table A.2- Mix no. 3

Mix No.	Cylinder No.	Rest period (hours)	Curing period (hours)	Curing temp. C°/F°	Age (days)	Compressive strength (psi)	Average (psi)
3-A	1	5 h	24 h	60/140	7 d	3,485	3,332
	2	5 h	24 h	60/140	7 d	3,574	
	3	5 h	24 h	60/140	7 d	2,937	
3-B	1	24 h	0 h	A*	1 d	335	351
	2	24 h	0 h	A*	1 d	367	
	3	24 h	0 h	A*	1 d	_	
3-C	1	24 h	48 h	60/140	3 d	3,182	3,106
	2	24 h	48 h	60/140	3 d	3,140	
	3	24 h	48 h	60/140	3 d	2,998	
3-D	1	24 h	24 h	60/140	3 d	3,030	3,051
	2	24 h	24 h	60/140	3 d	3,000	
	3	24 h	24 h	60/140	3 d	3,126	

- Aggregate: 1/2 inch, crushed dolomite
- Sodium Hydroxide solution: 14M
- Sodium Silicate: type N®
- All dry materials were mixed first, then chemicals and water were added
- HRWR: Gelinum-7500
- * Ambient temperature curing
- Slump flow: 23.5 in

Table A.3- Mix no. 4

Mix No.	Cylinder No.	Rest period (hours)	Curing period (hours)	Curing temp. C°/F°	Age (days)	Compressive strength (psi)	Average (psi)
4-A	1	_	24 h	60/140	3 d	3,510	3,483
	2	_	24 h	60/140	3 d	3,422	
	3	_	24 h	60/140	3 d	3,516	
4-B	1	_	24 h	60/140	7 d	3,638	3,673
	2	_	24 h	60/140	7 d	3,688	
	3	_	24 h	60/140	7 d	3,693	
4-C	1	_	24 h	60/140	28 d	3,379	3,640
	2	_	24 h	60/140	28 d	3,823	
	3	_	24 h	60/140	28 d	3,717	

- Aggregate: 1/2 inch, crushed dolomites
- Sodium Hydroxide solution: 16M
- Sodium Silicate: type D™
- All dry materials were mixed first, then chemicals and water were added
- HRWR: Gelinum-7500
- Slump flow: 23.5 in

Table A.4- Mix no. 5

Mix No.	Cylinder No.	Rest period (hours)	Curing period (hours)	Curing temp. C°/F°	Age (days)	Compressive strength (psi)	Average (psi)
5-A	1	_	24 h	60/140	1 d	3,937	3,899
	2	_	24 h	60/140	1 d	3,795	
	3	_	24 h	60/140	1 d	3,964	
5-B	1	_	24 h	60/140	3 d	4,054	4,040
	2	_	24 h	60/140	3 d	4,043	
	3	_	24 h	60/140	3 d	4,023	
5-C	1	_	24 h	60/140	7 d	4,115	4,200
	2	_	24 h	60/140	7 d	4,231	
	3	_	24 h	60/140	7 d	4,254	

- Aggregate: 1/2 inch, crushed dolomite
- Sodium Hydroxide solution: 14M
- Sodium Silicate: type D™
- All dry materials were mixed first, then chemicals and water were added
- HRWR: Gelinum-7500
- Slump flow: 23.5 in

Table A.5- Mix no. 6

Mix No.	Cylinder No.	Rest period (hours)	Curing period (hours)	Curing temp. C°/F°	Age (days)	Compressive strength (psi)	Average (psi)
6-A	1	_	24 h	60/140	3 d	4,761	4,761
	2	_	24 h	60/140	3 d	_	
	3	_	24 h	60/140	3 d	_	
6-A	1	_	24 h	60/140	7 d	5,186	4,998
	2	_	24 h	60/140	7 d	4,713	
	3	_	24 h	60/140	7 d	5,096	
6-B	1	_	24 h	60/140	28 d	4,969	5,058
	2	_	24 h	60/140	28 d	5,063	
	3	_	24 h	60/140	28 d	5,142	
6-C	1	_	24 h	60/140	100 d	5,311	5,282
	2	_	24 h	60/140	100 d	5,068	
	3	_	24 h	60/140	100 d	5,466	

- Aggregates: 1/2 inch, crushed dolomites
- Sodium Hydroxide solution: 14M
- Sodium Silicate: type D™
- Fly ash and chemicals were mixed first, then dry materials were added
- HRWR: Gelinum-7500
- Slump flow: 23 in

Table A.6- Mix no.7

Mix No.	Cylinder No.	Rest period (hours)	Curing period (hours)	Curing temp. C°/F°	Age (days)	Compressive strength (psi)	Average (psi)
7-A	1	_	24 h	65/150	1 d	4,667	4,606
	2	_	24 h	65/150	1 d	4,691	
	3	_	24 h	65/150	1 d	4,460	
7-B	1	_	24 h	65/150	7 d	4,719	4,851
	2	_	24 h	65/150	7 d	4,983	
	3	_	24 h	65/150	7 d	_	
7-C	1	_	24 h	65/150	28 d	5,081	5,153
	2	_	24 h	65/150	28 d	5,173	
	3	_	24 h	65/150	28 d	5,205	
						Modulus of elasticity (psi)	
7-D	1	_	24 h	65/150	28 d	4,500,000	4,500,000
	2	_	24 h	65/150	28 d	_	
	3	_	24 h	65/150	28 d	_	
						Splitting tensile strength (psi)	
7-E	1	_	24 h	65/150	28 d	402	383
	2	_	24 h	65/150	28 d	366	
	3	_	24 h	65/150	28 d	381	

- Aggregates: 1/2 inch, crushed dolomite
- Sodium Hydroxide solution: 14M
- Sodium Silicate: type N®
- Fly ash and chemicals were mixed first, then dry materials were added
- No HRWR added
- Slump flow: 20 in

Table A.7- Mix no. 8

Mix No.	Cylinder No.	Rest period (hours)	Curing period (hours)	Curing temp. C°/F°	Age (days)	Comp. strength (psi)	Average (psi)
8-A	1	_	24 h	65/150	1 d	5,667	5,575
	2	_	24 h	65/150	1 d	5,603	
	3	_	24 h	65/150	1 d	5,454	
8-B	1	_	24 h	65/150	7 d	5,965	5,960
	2	_	24 h	65/150	7 d	5,955	
	3	_	24 h	65/150	7 d	_	
8-C	1	_	24 h	65/150	28 d	5,936	5,922
	2	_	24 h	65/150	28 d	5,878	
	3	_	24 h	65/150	28 d	5,953	
						Modulus of elasticity (psi)	
8-D	1	_	24 h	65/150	28 d	3,800,000	4,200,000
	2	_	24 h	65/150	28 d	4,600,000	
	3	_	24 h	65/150	28 d	_	
						Splitting tensile strength (psi)	
8-E	1	_	24 h	65/150	28 d	405	421
	2	_	24 h	65/150	28 d	444	
	3	_	24 h	65/150	28 d	414	

- Aggregates: 1/2 inch, crushed dolomite
- Sodium Hydroxide solution: 14M
- Sodium Silicate: type N®
- Fly ash and chemicals were mixed first, then dry materials were added
- No extra-added water
- Slump flow: 17 in

APPENDIX B

COMPRESSIVE STRENGTH OF TESTED (GC) BEAMS (THIRD DAY OF AGE)

Table B.1- Compressive strength of tested beams at 3 days

Beam ID	Cylinder No.	Age (days)	Compressive strength (psi)	Average (psi)
GL6-2.4	1	3 d	5,786	5,786
	2	3 d	-	
	3	3 d	-	
GL6-2	1	3 d	5,764	5,868
	2	3 d	5,929	
	3	3 d	5,911	
GS6-2	1	3 d	5,235	5,341
	2	3 d	5,302	
	3	3 d	5,486	
GN6-2	1	3 d	4,904	4,946
	2	3 d	4,848	
	3	3 d	5,085	
GN4-2	1	3 d	3,800	3,838
	2	3 d	3,970	
	3	3 d	3,745	

APPENDIX C

COMPARARISON OF TWO TYPES OF FLY ASH

Table C.1- Chemical composition of (Class F) fly ash

Component	Type 2 (%)	Type 1(%)
SiO_2[1]	59.27	48.28
Al_2O_3[2]	22.09	20.14
Fe_2O_3[3]	5.15	15.22
Sum of [1'2'3]	86.51	83.63
CaO	8.30	7.49
MgO	1.62	1.07
SO_3	0.44	2.41
Na_2O	0.15	0.92
K_2O	1.08	-
LOI	0.30	1.14

Type 2: Successful mix

Type 1: Unsuccessful mix

Table C.2- Physical properties of (Class F) fly ash

	Type 2[a]	Type 1[b]
Retained on #325 Sieve, %	29.22	14.1
Specific Gravity	2.25	2.45
Moisture Content, %	0.03	0.12

[a] Successful mix

[b] Unsuccessful mix

Figure C.1- Flash setting of the unsuccessful mix (FA Type 1)

Figure C.2- Flash setting of the unsuccessful mix (FA unknown source)

APPENDIX D

STRAIN GAUGE READINGS OF TESTED BEAMS

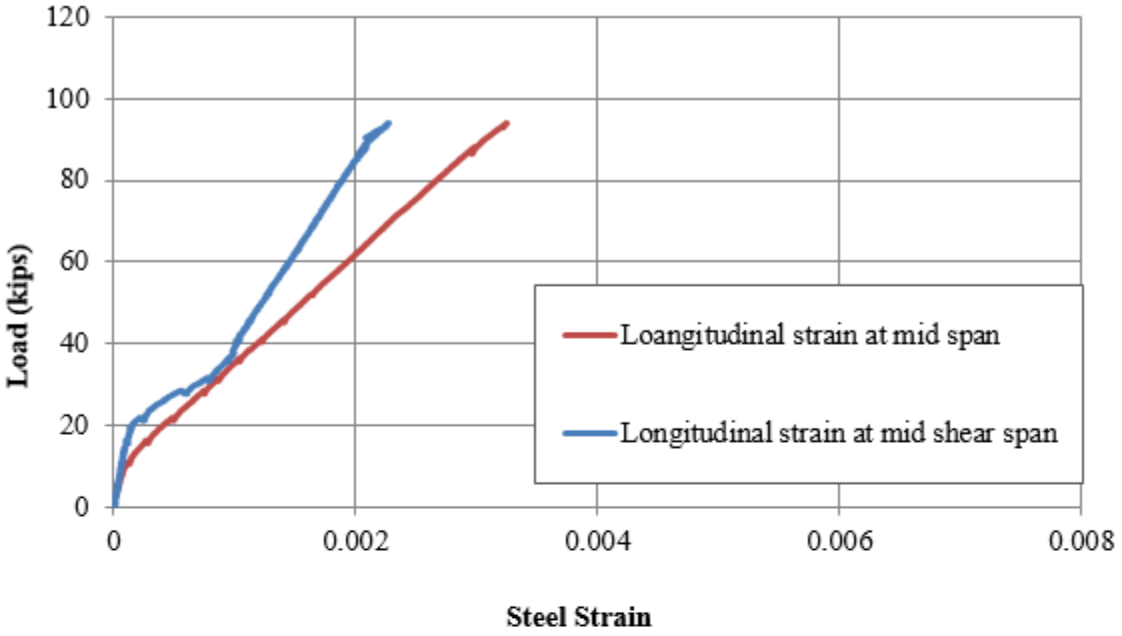

(a) East side of the beam

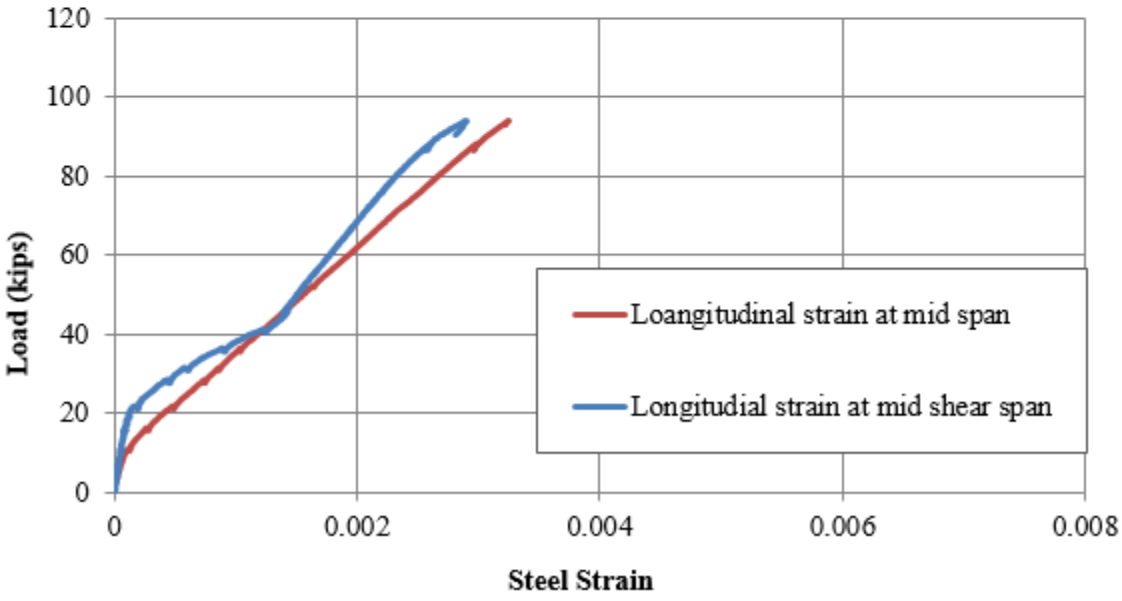

(b) West side of the beam

Figure D.1- Load—strain curve of GN6-2

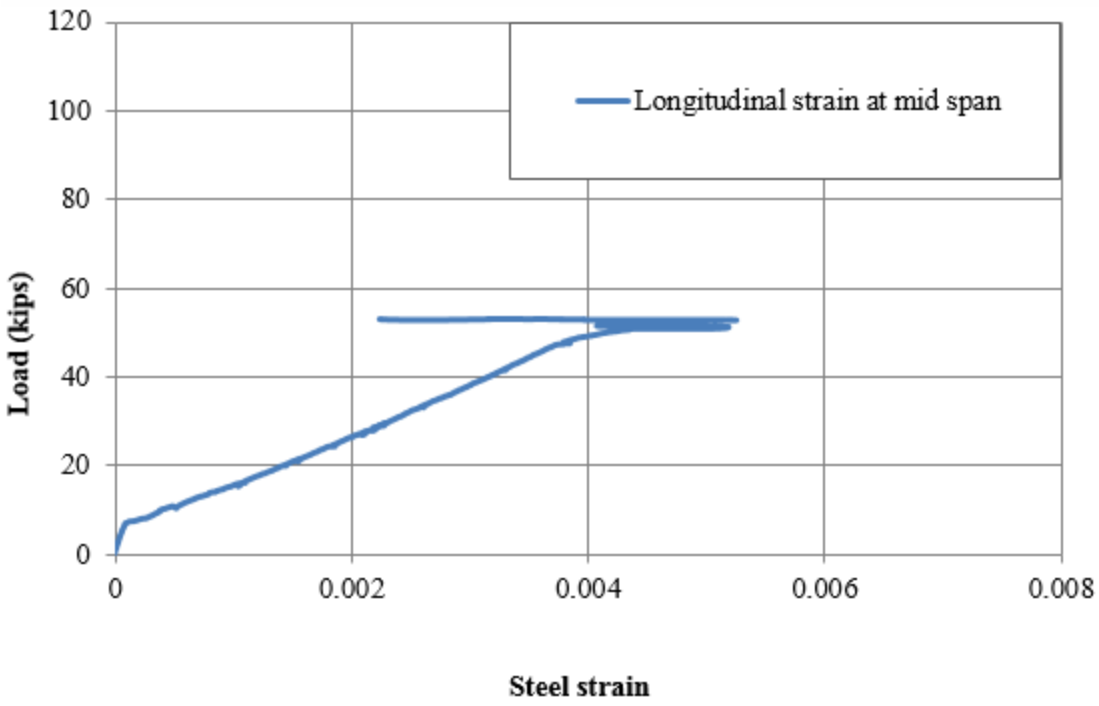

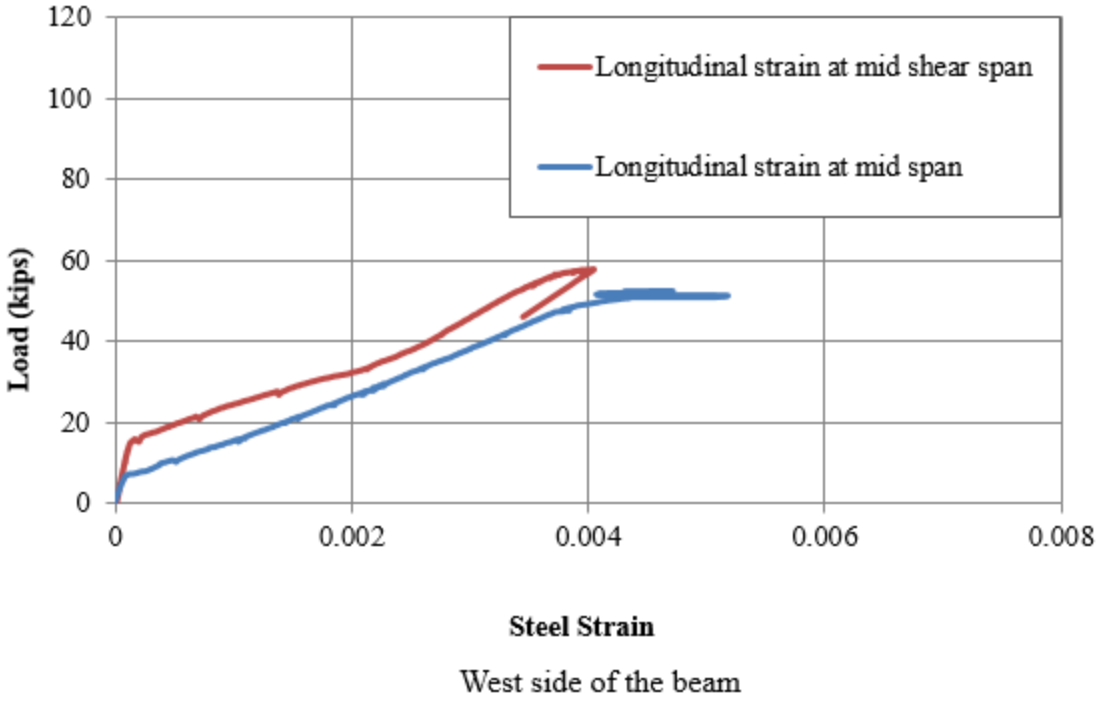

Figure D.2- Load—strain curve of GN4-2

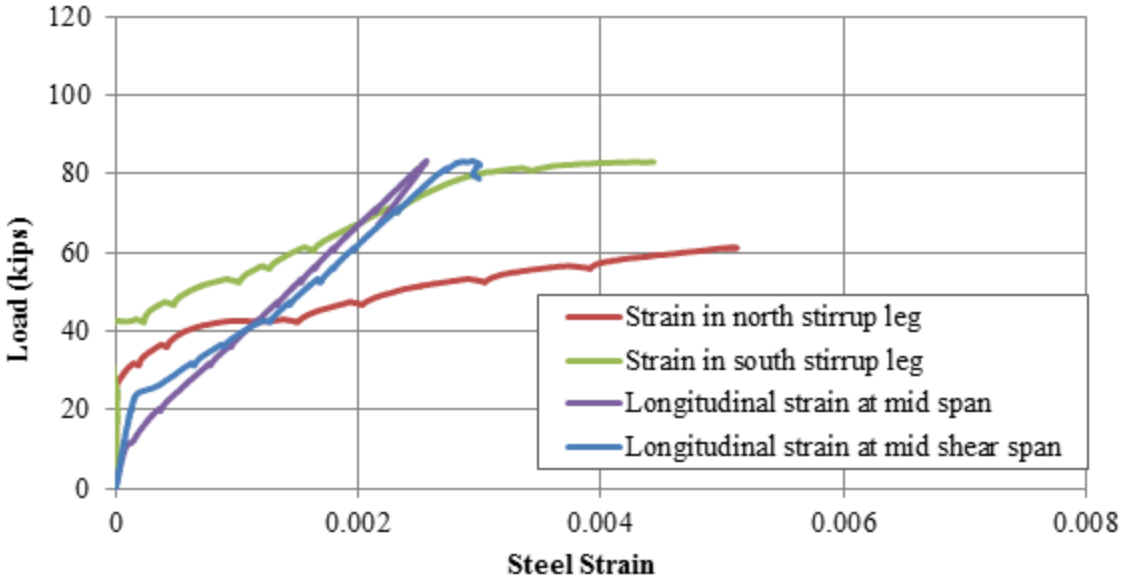

(a) East side ot the beam)

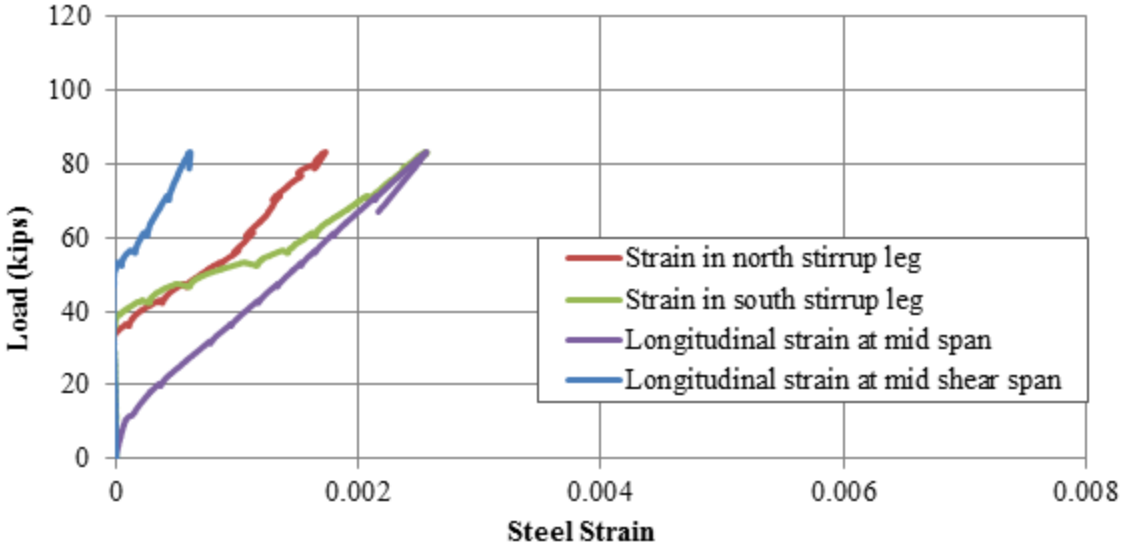

(b) West side of the beam

Figure D.3- Load—strain curve of GL6-2

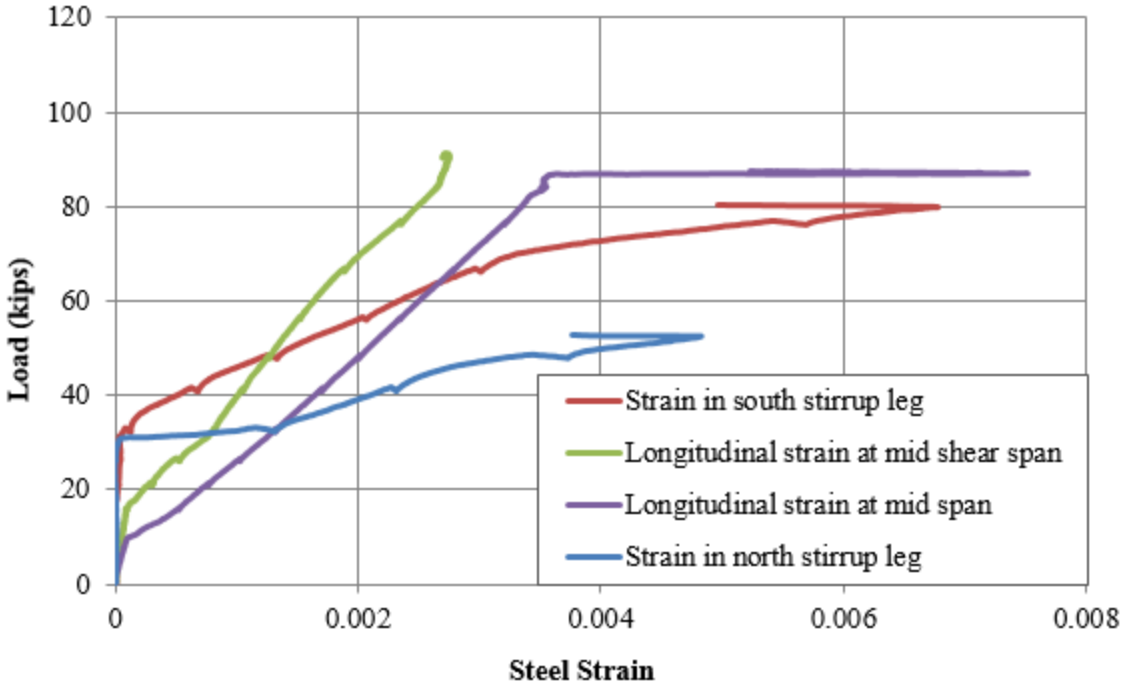

(a) East side fo the beam

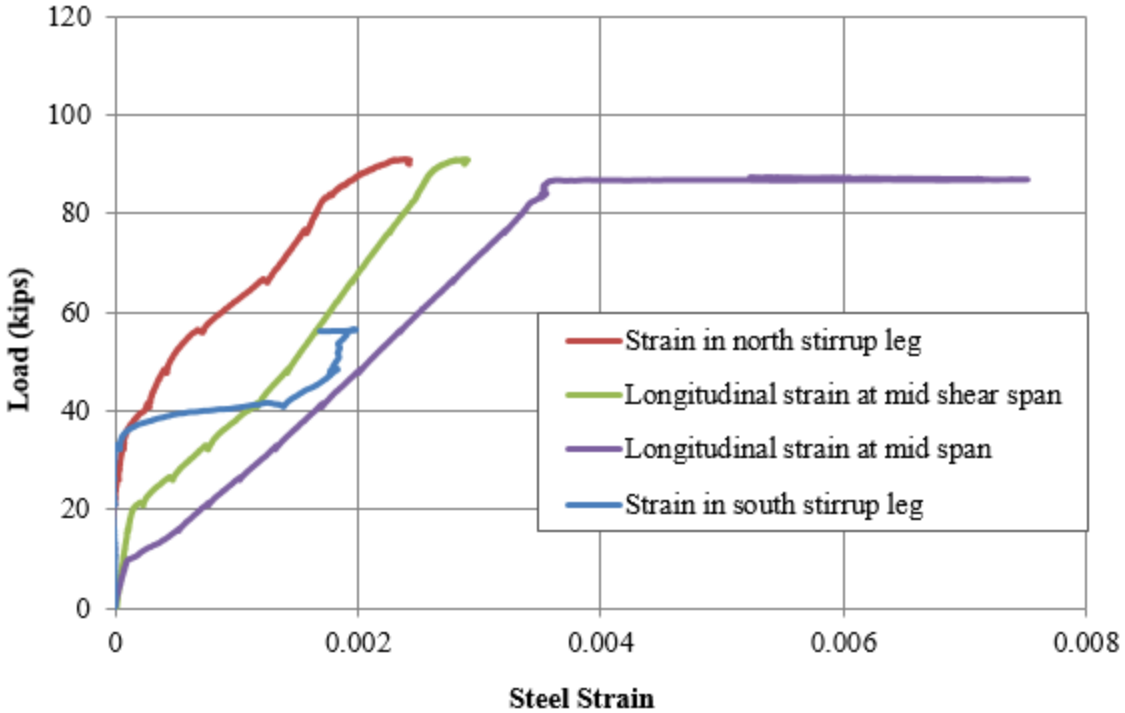

(b) West side of the beam

Figure D.4- Load—strain curve of GL6-2.4

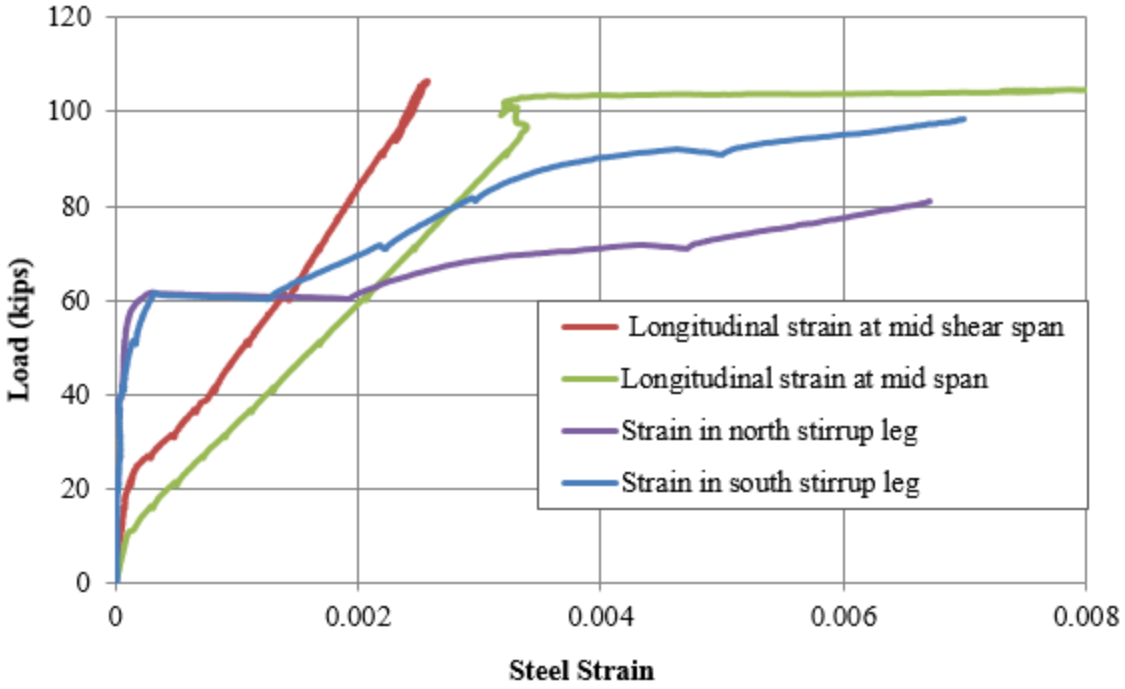

(a) East side of the beam

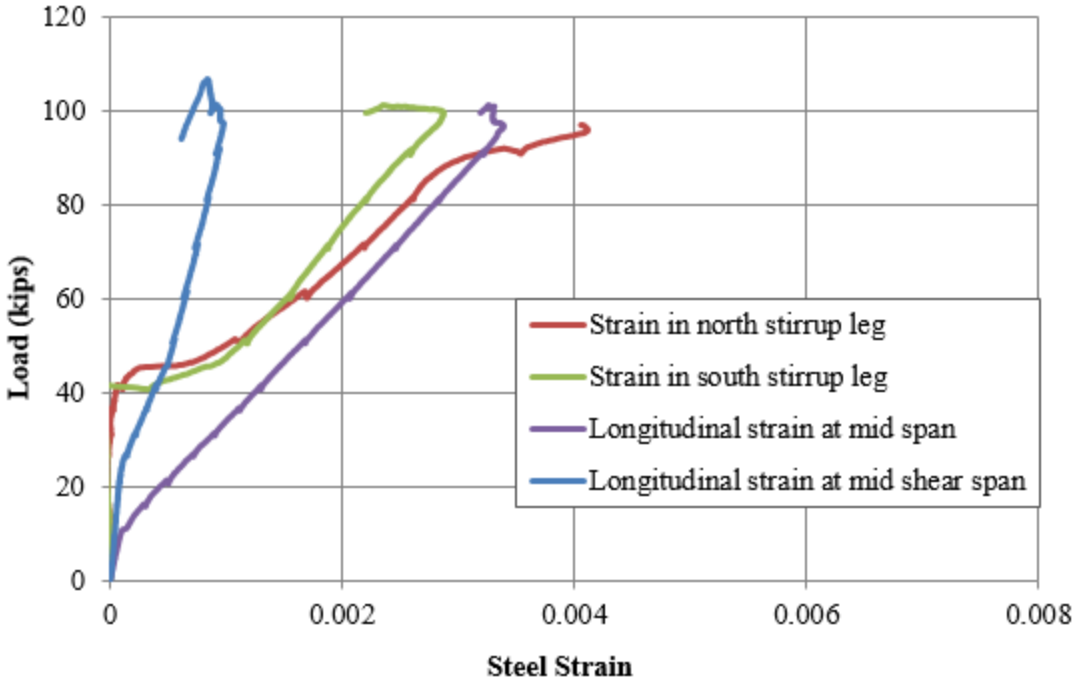

(b) West side of the beam

Figure D.5- Load—strain curve of GS6-2

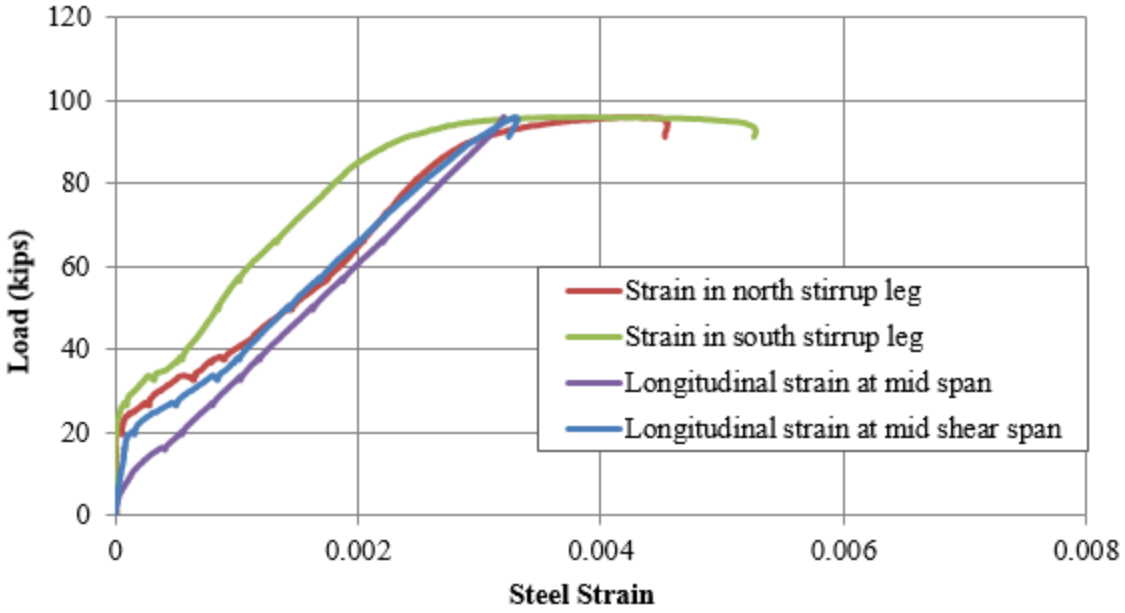

(a) East side of the beam

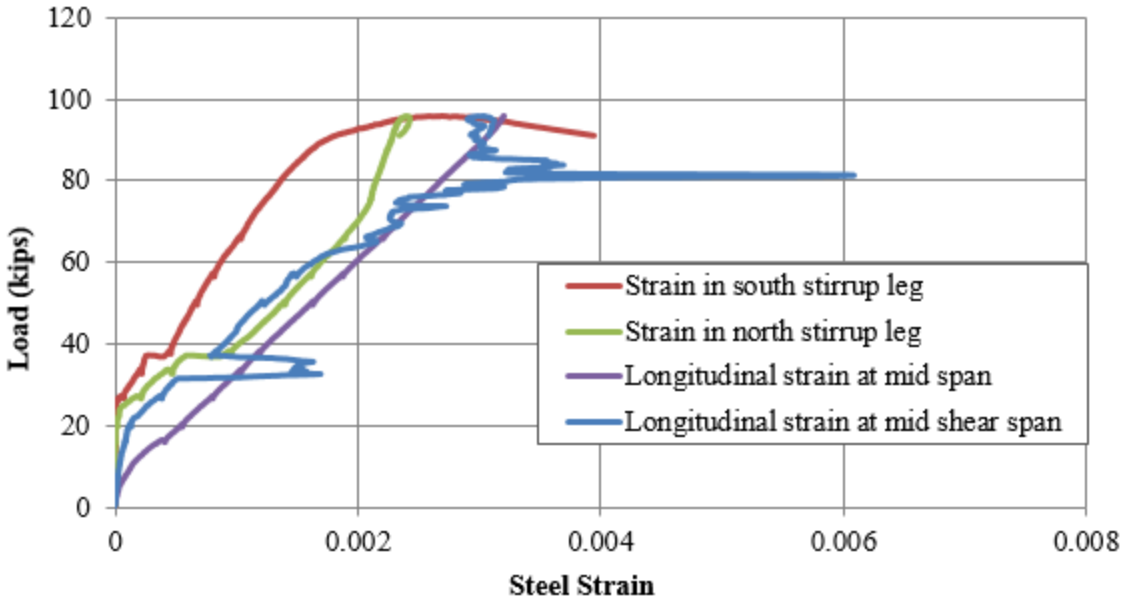

(b) West side of the beam

Figure D.6- Load—strain curve of CL6-2

APPENDIX E

AVERAGE CONCRETE STRAIN IN TESTED BEAMS

The average concrete strain is defined in the next curves as the LVDT reading divided by the length between the tip and the fixation point of the LVDT. These appendix illustrations show the average concrete strain in the direction of the compression stud (Figure E.1), the direction of tensile stress across diagonal crack (Figure E.2), and the direction of longitudinal strain on top and bottom of the beam (Figure E.3), all versus shear stress. Note that the compression strain in Figure E.1 is taken as negative sign.

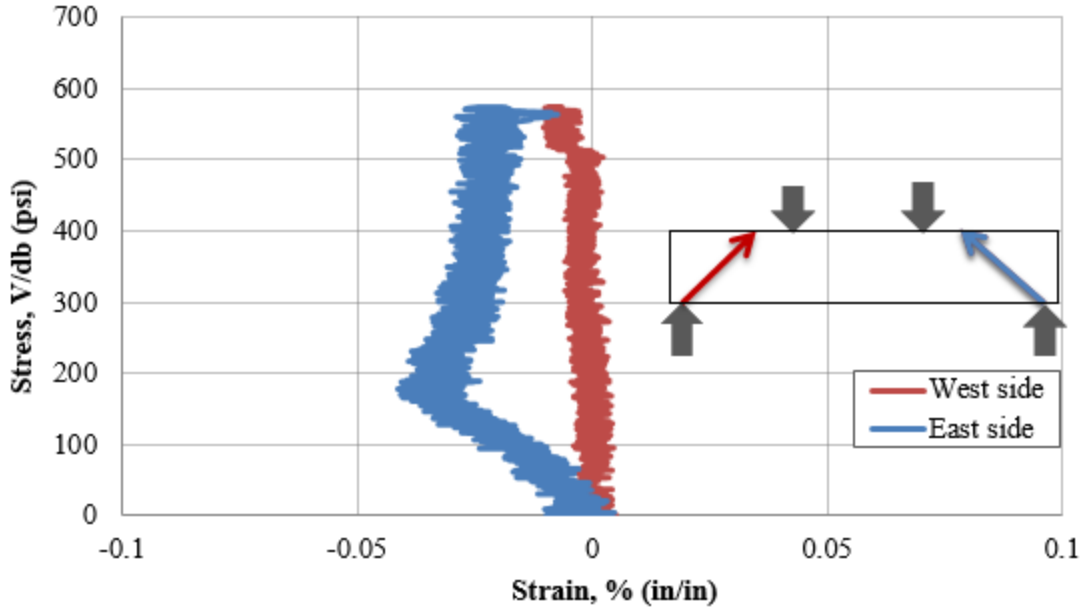

(a) GN6-2

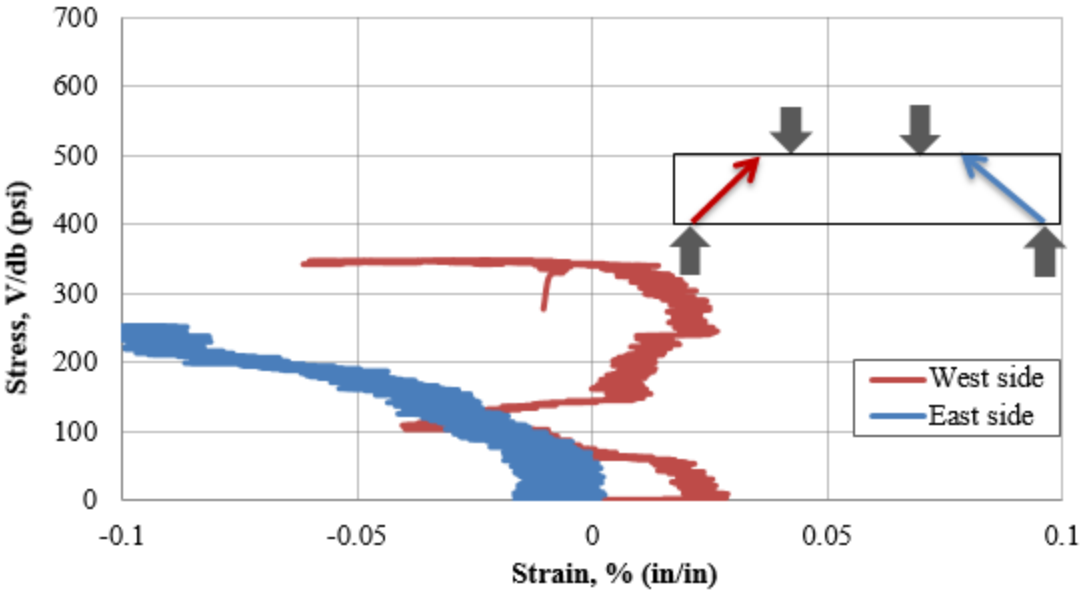

(b) GN4-2

Figure E.1- Average strain in compression stud of the tested beams versus stress

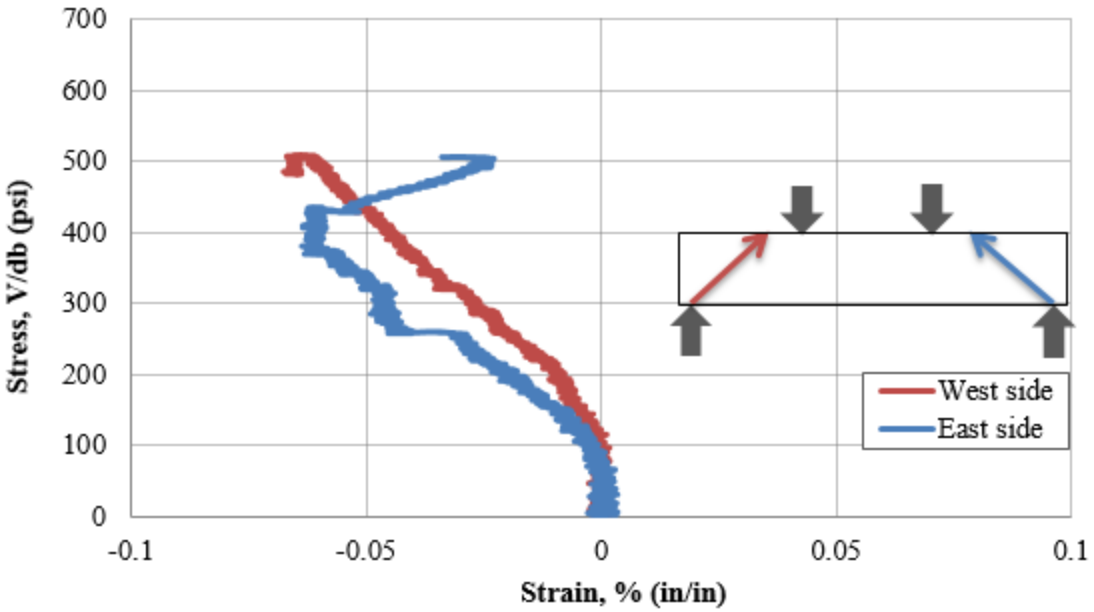

(c) GL6-2

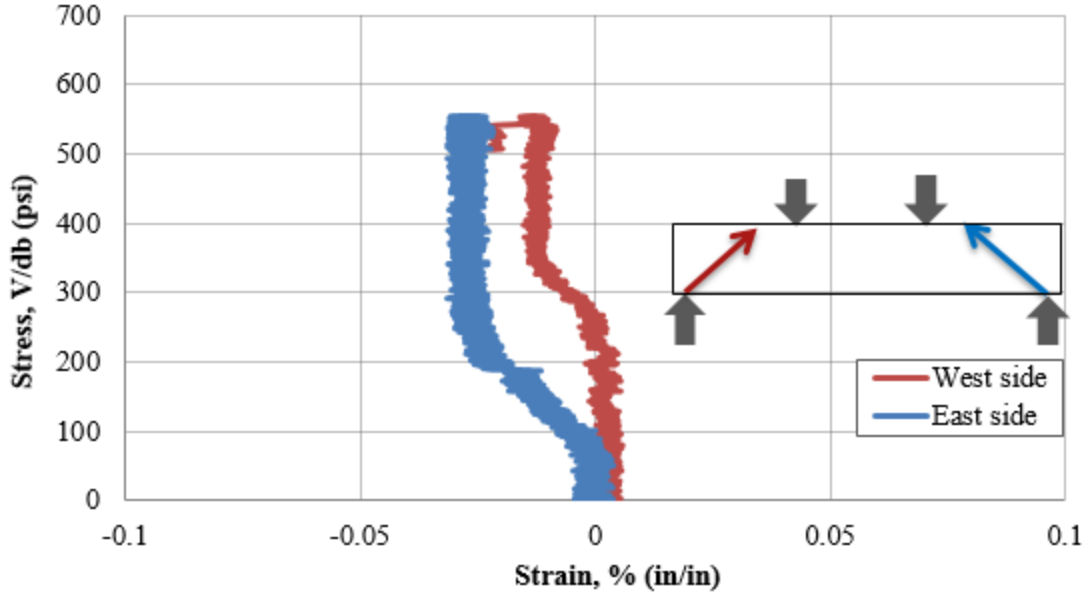

(d) GL6-2.4

Figure E.1- Average strain in compression stud of the tested beams versus stress (cont.)

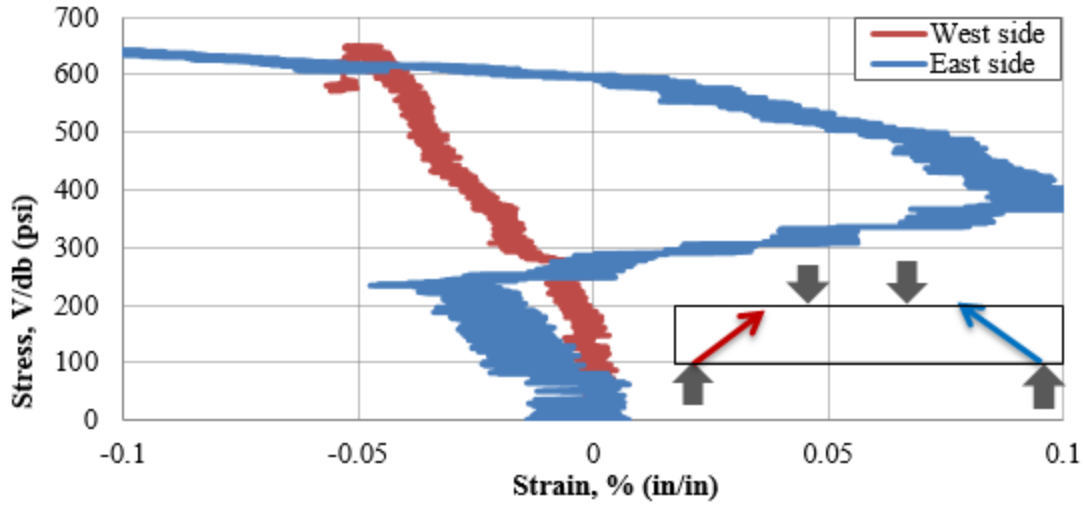

(e) GS6-2

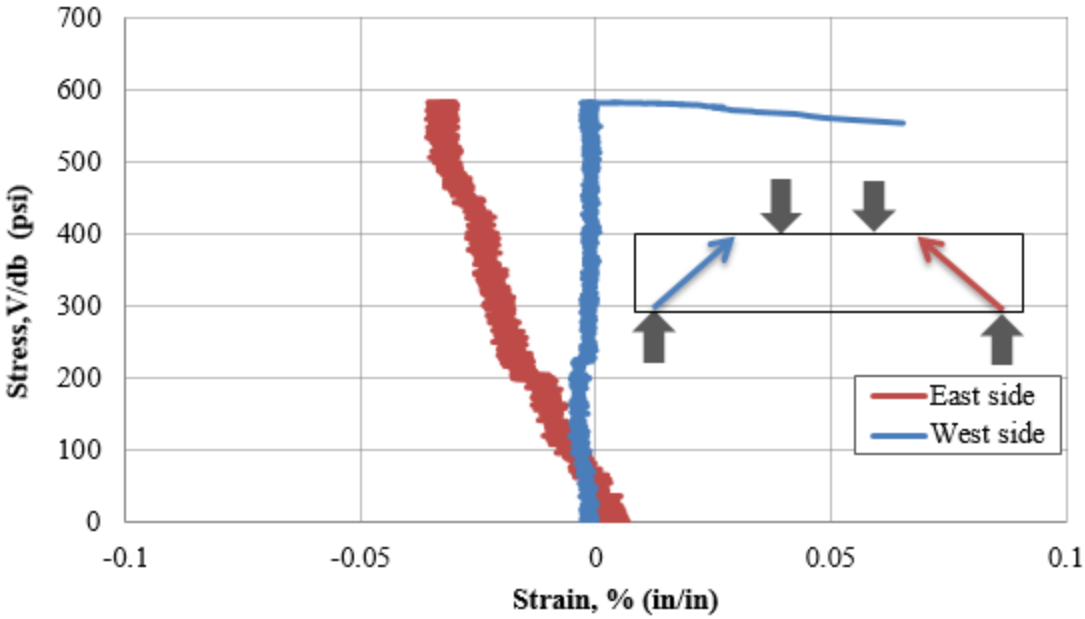

(f) CL6-2

Figure E.1- Average strain in compression stud of the tested beams versus stress (cont.)

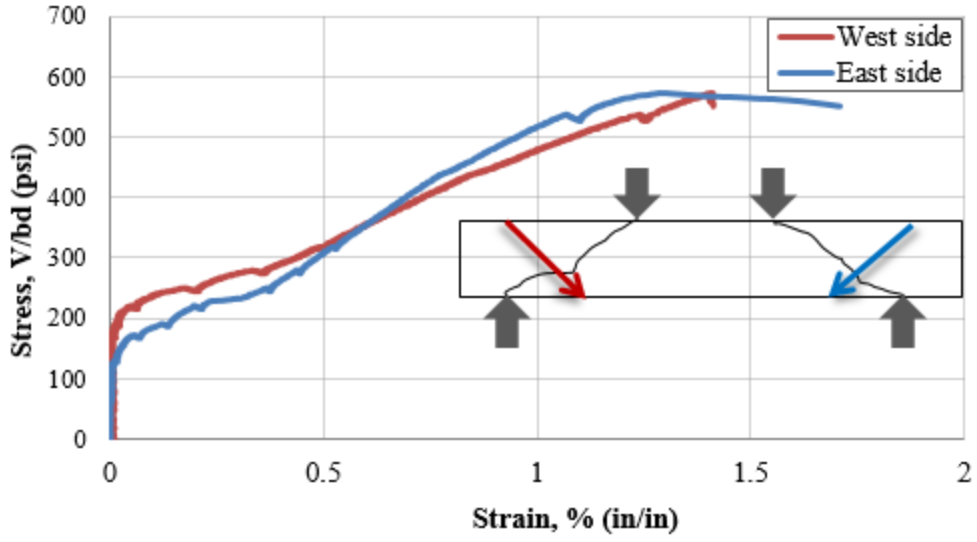

(a) GN6-2

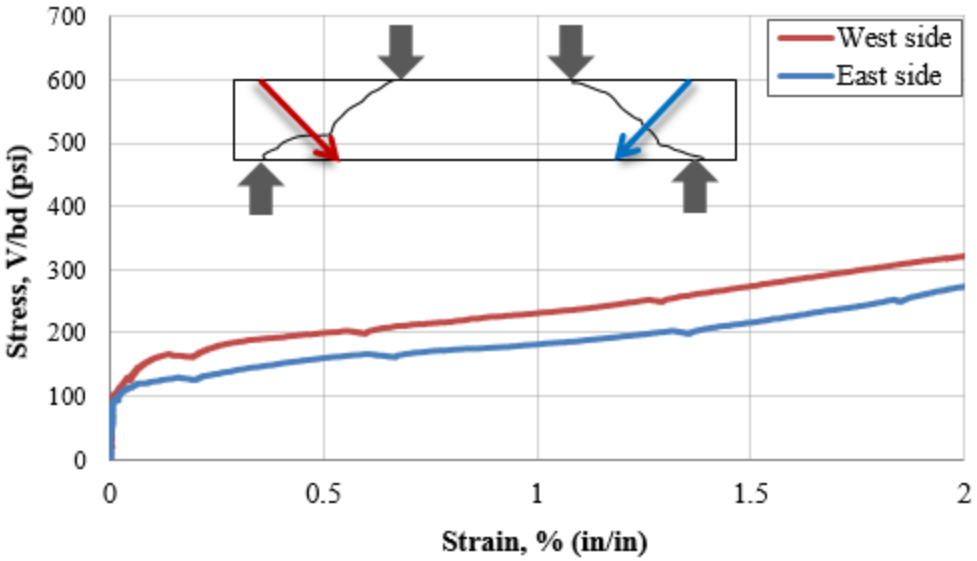

(b) GN4-2

Figure E.2- Average strain across the diagonal crack of the tested beams versus stress

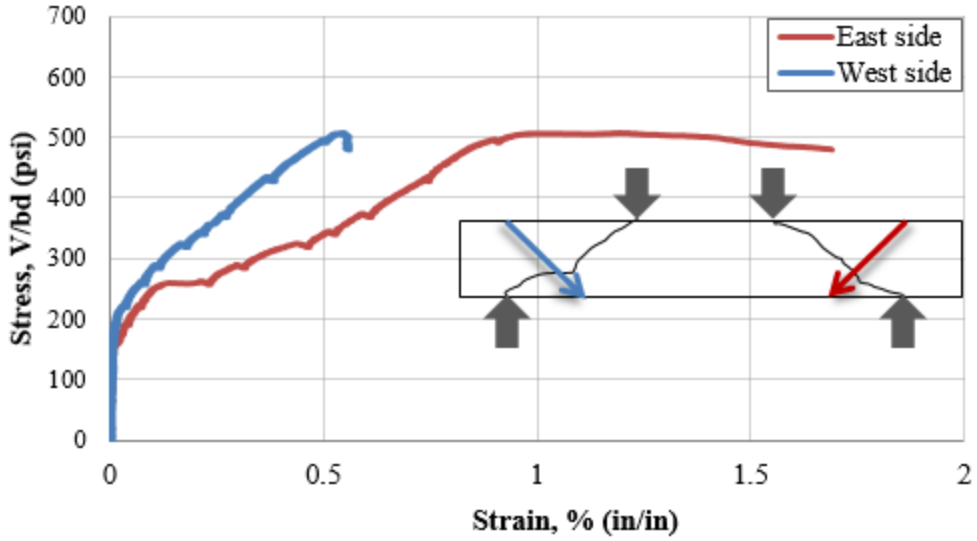

(c) GL6-2

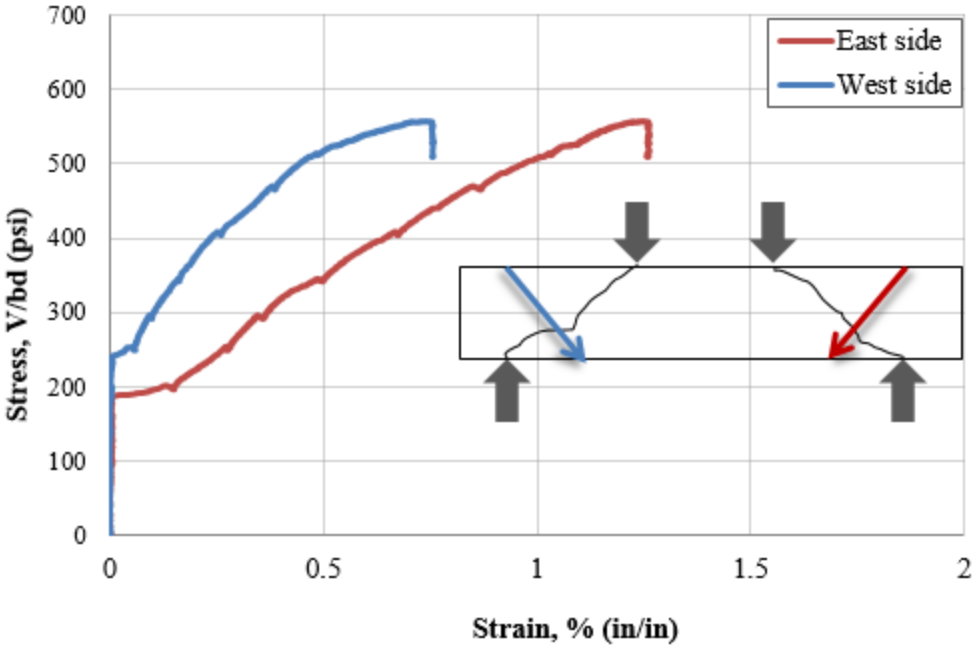

(d) GL6-2.4

Figure E.2- Average strain across the diagonal crack of the tested beams versus stress (cont.)

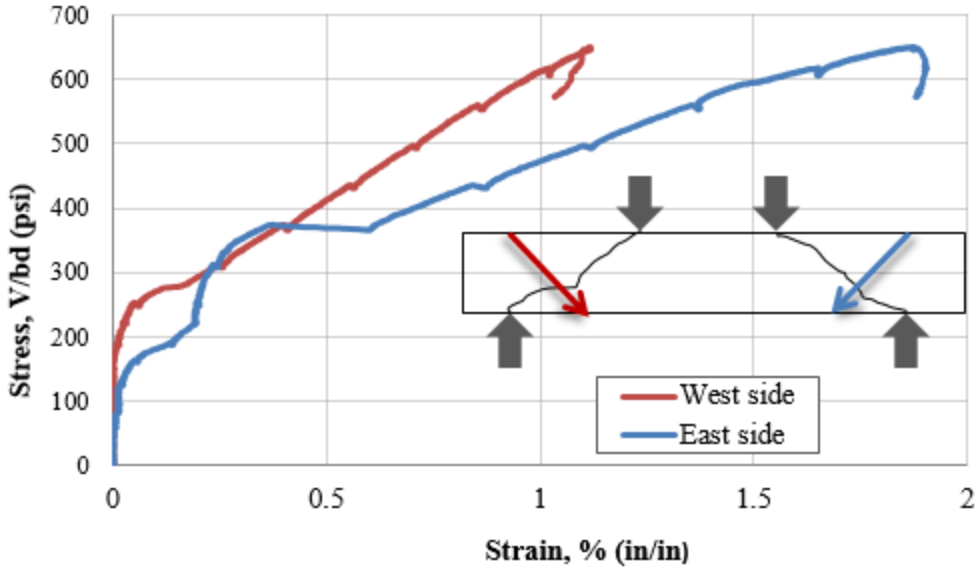

(e) GS6-2

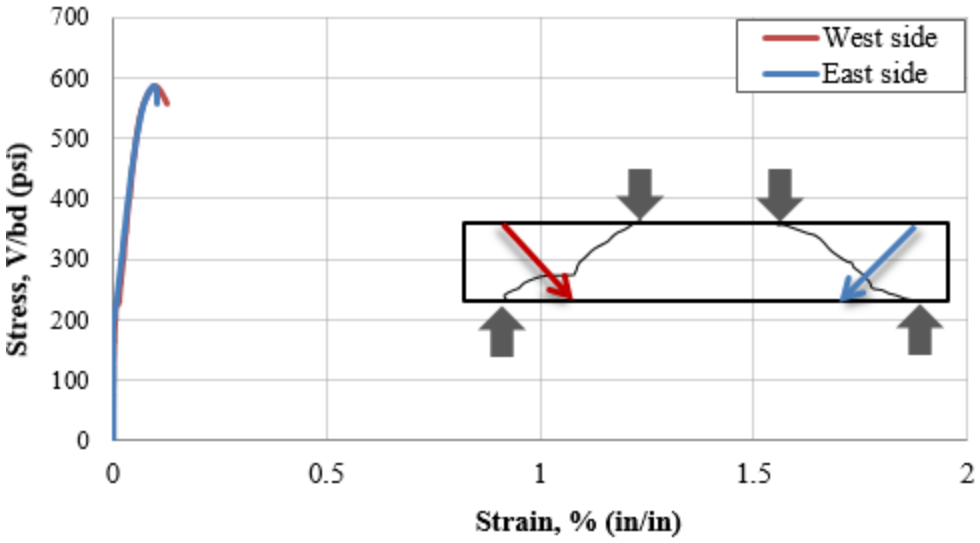

(f) CL6-2

Figure E.2- Average strain across the diagonal crack of the tested beams versus stress (cont.)

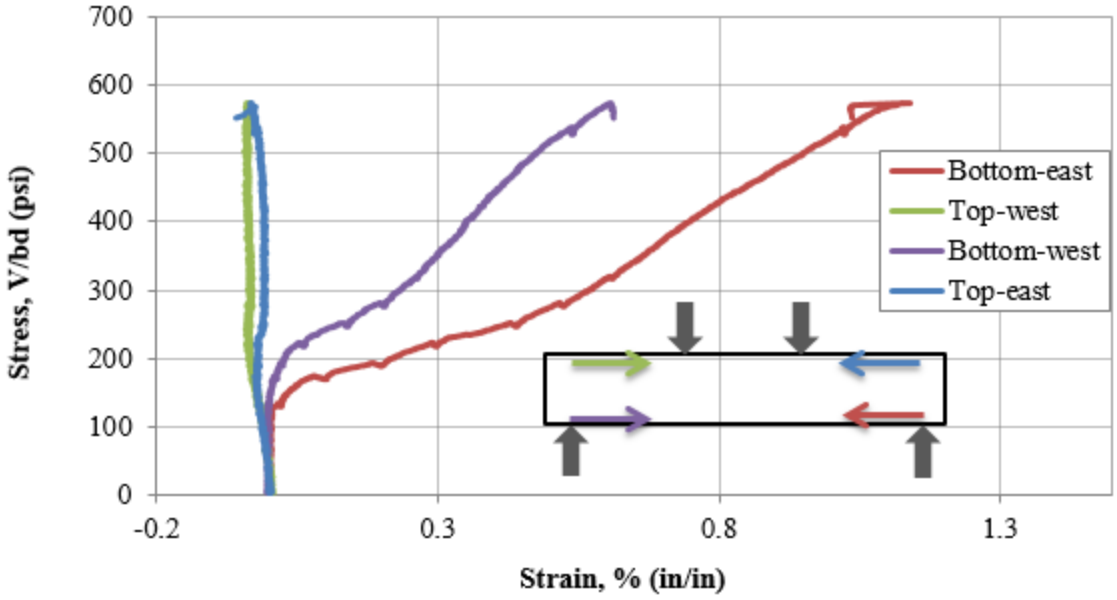

(a) GN6-2

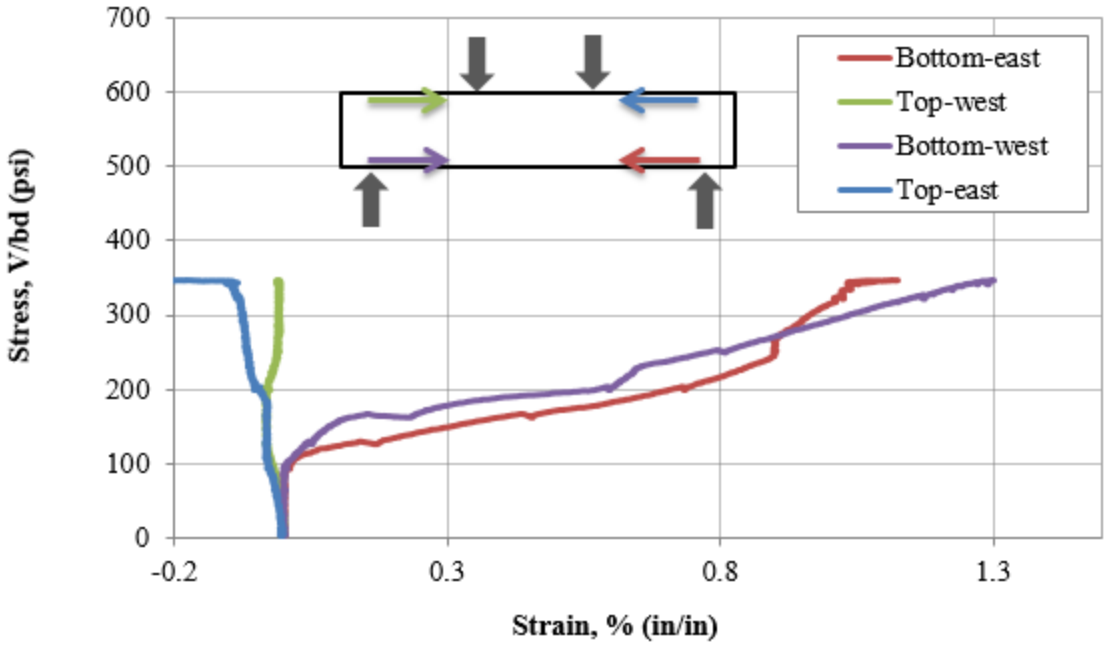

(b) GN4-2

Figure E.3- Average strain in the longitudinal direction of the tested beams versus stress

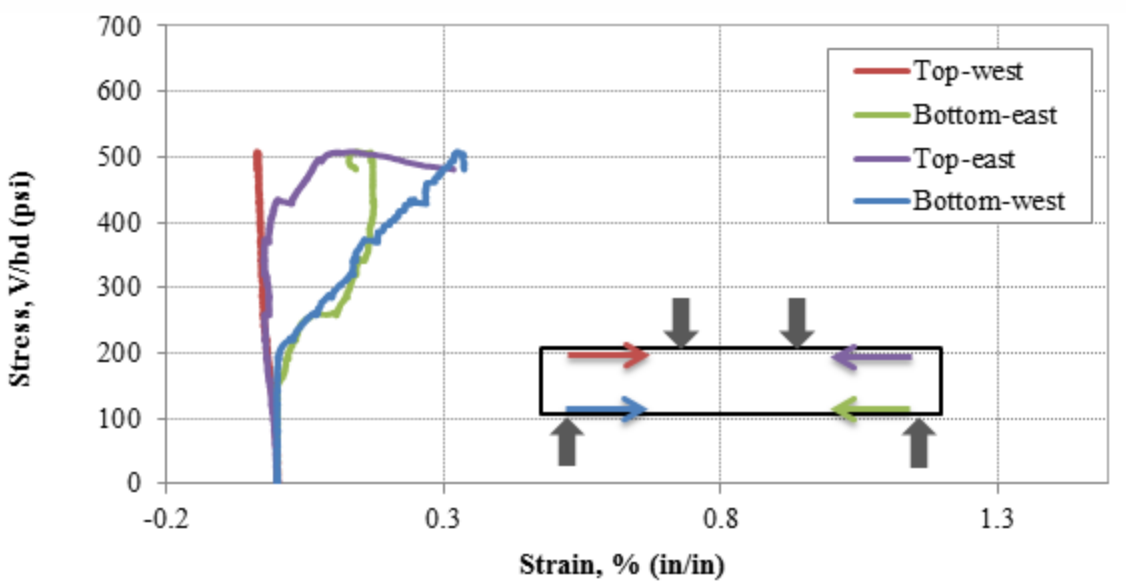

(c) GL6-2

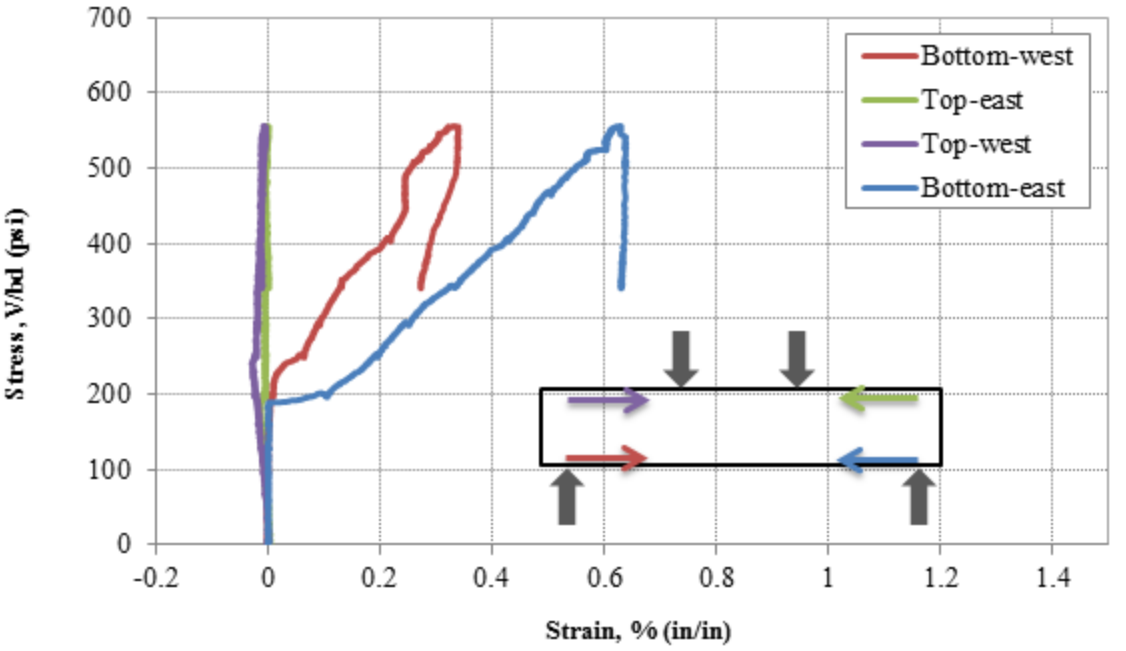

(d) GL6-2.4

Figure E.3- Average strain in the longitudinal direction of the tested beams versus stress (cont.)

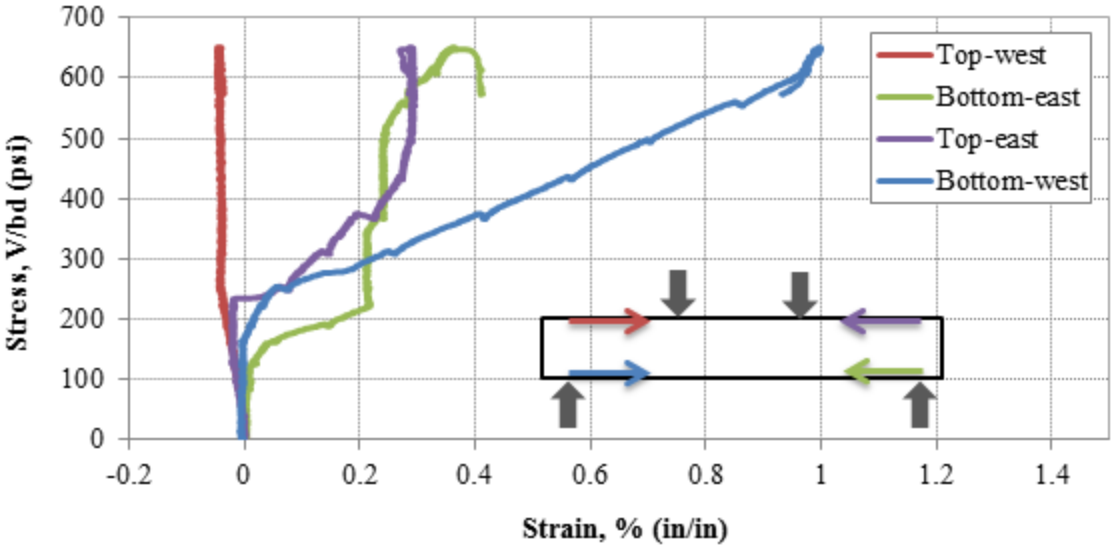

(e) GS6-2

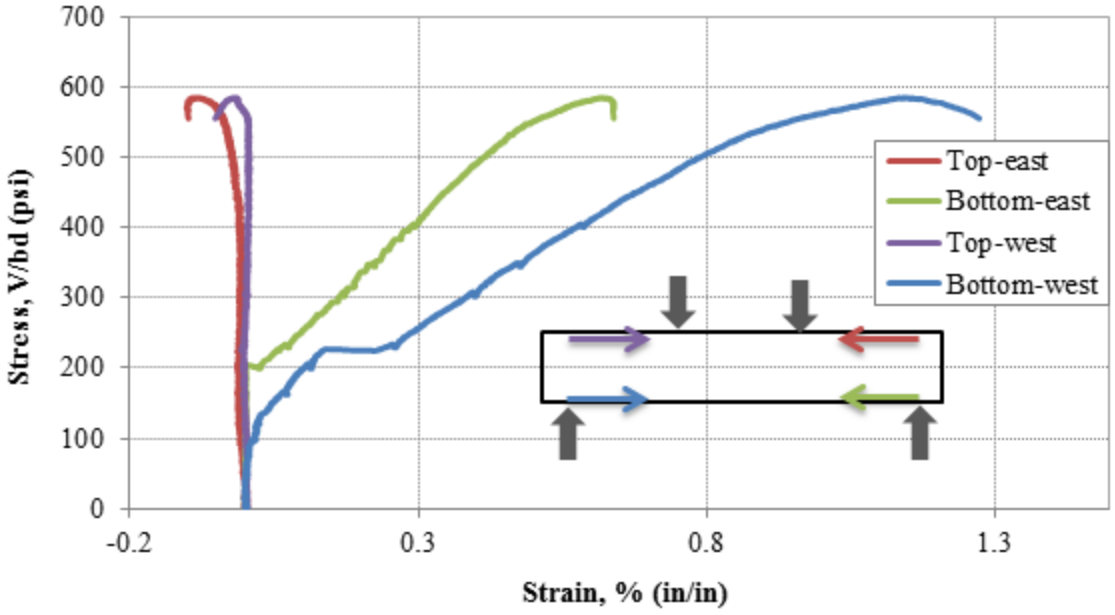

(f) CL6-2

Figure E.3- Average strain in the longitudinal direction of the tested beams versus stress (cont.)

APPENDIX F

THERMOCOUPLE READINGS OF THE TESTD BEAMS

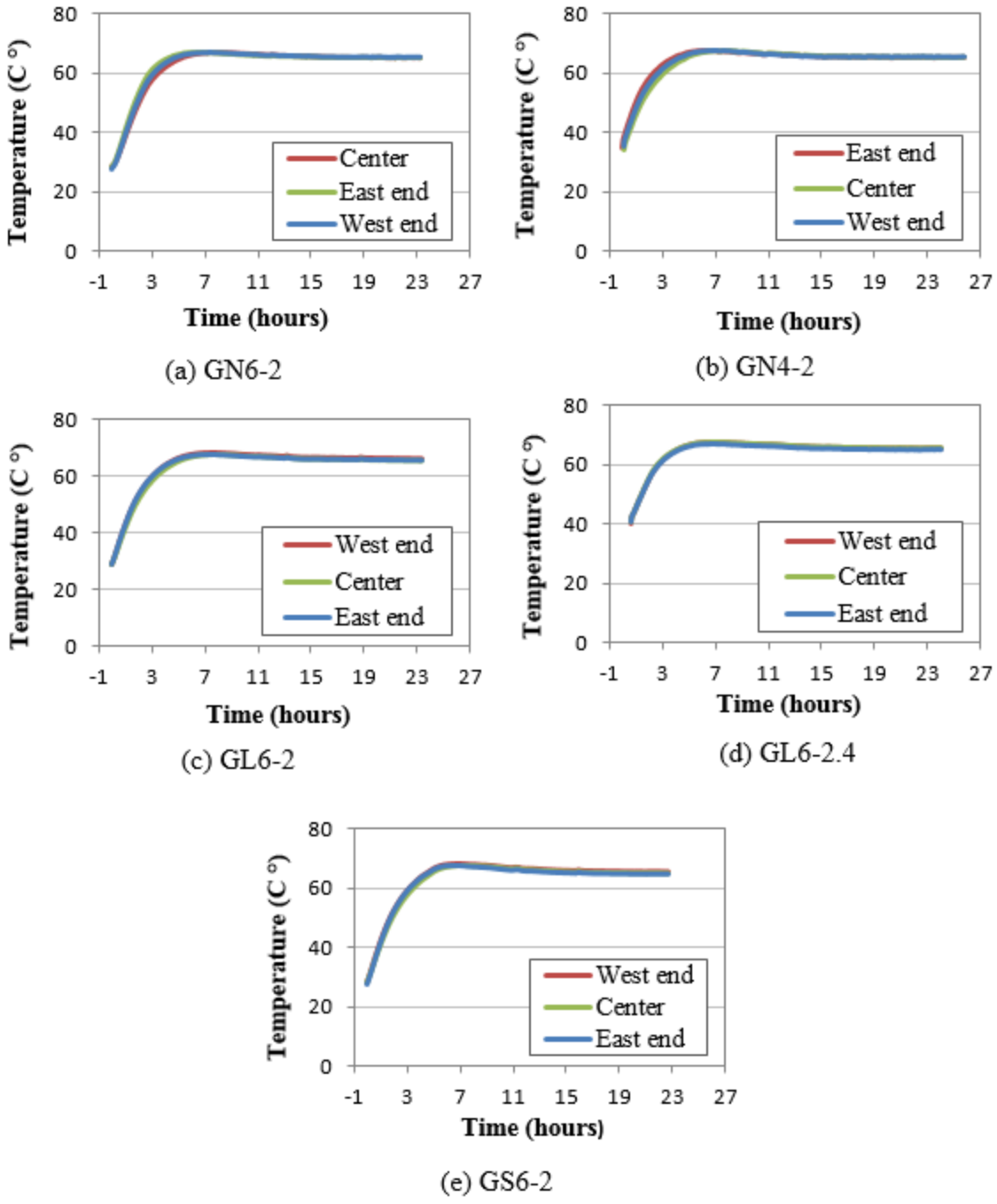

Figure F.1- Thermocouple readings of the tested beams

APPENDIX G

CLAUSES AND NOTATIONS OF DIFFERENT INTERNATIONAL STANDARDS

Table G.1- Standards provisions of shear strength

AASHTO LRFD (2010)	
5.8.3.3 Nominal Shear Resistance The nominal shear resistance, Vn for nonprestressed members shall be determined by, $$V_n = V_c + V_s$$ in which: $$V_c = 0.0316\beta\sqrt{f'_c}\,b_v d_v$$ if the procedures of article 5.8.3.4.2 is used, and, $$V_s = \frac{A_v f_y d_v \cot\theta}{s} \quad for\ \alpha = 90^{\circ}$$ **5.8.3.4.2 General Procedure** For members not subjected to axial load, $$\beta = \frac{4.8}{(1 + 750\varepsilon_s)}$$ • If the section contains at least the minimum amount of transverse reinforcement, and $$\beta = \frac{4.8}{(1 + 750\varepsilon_s)}\frac{51}{(39 + S_{xe})}$$ • If the section contains less than the minimum amount of transverse reinforcement $$\varepsilon_s = \frac{\frac{|M_u|}{d_v} + V_u}{E_s A_s}$$ $$S_{xe} = S_x \frac{1.38}{a_g + 0.63}$$	where: $b_v = effective\ web\ width\ , (in.)$ $d_v = effective\ shear\ depth, 0.9d, (in)$ $s = spacing\ of\ stirrups\ (in)$ $\beta = factor\ indicating\ ability\ of\ diagonally\ cracked\ concrete\ to\ transmit\ tension\ and\ shear$ $\theta = angle\ of\ inclination\ fo\ diagonal\ compressive\ stresses\ (°)$ $\alpha = angle\ of\ inclination\ of\ stirrups\ to\ Longitudinal\ axis\ (°)$ $A_v = area\ of\ shear\ reinforcement\ within\ a\ distance\ s\ (in^2)$ $f'_c = concrete\ compressive\ strenght\ (ksi)$ $A_s = area\ of\ nonprestressed\ steel\ on\ the\ flexural\ tension\ side\ of\ the\ member\ at\ the\ section\ under\ consideration$ $M_u = factored\ moment(kip - in)$ $V_u = factored\ shear\ force\ (kip)$ $E_s = Modulus\ of\ elasticity\ of\ longitudinal\ Reinforcement\ (ksi)$ $S_x = d_v$ $a_g = max.size\ of\ aggregate(in)$

Table G.1- Standards provisions of shear strength (cont.)

ACI 318 (2011) Eq. (11-5) & Eq. (11-3)	
11.2 - Shear strength provided by concrete for nonprestressed members 11.2.2.1 - For members subject to shear and flexure only, $V_c = \left(1.9\lambda\sqrt{f'_c} + 2500\rho_w \frac{V_u d}{M_u}\right) b_w d$ (11-5) but not greater than 3.5λ *bwd*. When computing *Vc* by Eq. (11-5), *Vud* / *Mu* shall not be taken greater than 1.0, where *Mu* occurs simultaneously with *Vu* at section considered. **11.4 - Shear strength provided by shear reinforcement** 11.4.7.2 - Where shear reinforcement perpendicular to axis of member is used, $V_s = \frac{A_v f_{yt} d}{s} \qquad (11-15)$ where *Av* is the area of shear reinforcement within spacing *s*. 11.2.1.1 - For members subject to shear and flexure only, $V_c = 2\lambda\sqrt{f'_c} b_w d \qquad (11-3)$	Where: $V_n = nominal\ shear\ strength, lb$ V_c =*nominal shear strength provided byconcrete, lb* V_s =*nominal shear strength provided by shear reinforcement, lb* λ =*modification factor reflecting the reduced mechanical properties of lightweight concrete* f'_c =*specified compressive strength of concrete, psi,* $\rho_w = ratio\ of\ A_s\ to\ b_w d$ $V_u = factored\ shear\ force\ at\ section, lb$ M_u=*factored moment at section, in.-lb* $b_w = web\ width, in.$ *d= distance from extreme compression fiber to centroid of longitudinal tension reinforcement, in.* A_v=*area of shear reinforcement spacing s, in.2* f_{yt} =*specified yield strength fy of transvers reinforcement, psi*

Table G.1- Standards provisions of shear strength (cont.)

AS 3600 (2009)	
8.2.7 Shear strength of a beam excluding shear reinforcement The design shear strength of a beam shall be taken as φV_u where, $V_u = V_{uc} + V_{us}$ $(AS\ 8.2.2)$ V_{uc} is determined by, $V_{uc} = \beta_1\beta_2\beta_3 b_v d_\circ f_{cv}$ $(AS\ 8.2.7.1)$ **8.2.10 Contribution to shear strength by the shear reinforcement** V_{us} is determined by, $V_{us} = \frac{A_{sv} f_{sy.f} d_\circ \cot\theta_v}{s}$ $(AS\ 8.2.10)$ where: $V_u = shear\ strength\ (N)$ $if\ A_{sv} \geq A_{sv-min}\ then$ $\beta_1 = 1.1\left(1.6 - \frac{d_\circ}{1000}\right) \geq 1.1$ $otherwise\ \beta_1 = 1.1\left(1.6 - \frac{d_\circ}{1000}\right) \geq 0.8$ $\beta_2 = 1$ $for\ members\ subjected\ to\ pure\ bending$ $\beta_3 = 1\ or\ \frac{2d_\circ}{a_v} \leq 2$ $In\ case\ of\ diagonal\ compression\ over\ a_v$	Where: $f_{cv} = f'^{\frac{1}{3}}_c \leq 4\ MPa$ $b_v = effective\ width\ of\ a\ web\ for\ shear\ (mm)$ $d_\circ =$ *distance from the extreme compressive fiber of the concrete to the centroid of the outermost layer of tensile reinforcement (mm)* $A_{st} =$*cross-sectional area of longitudinal tensile reinforcement* (mm^2) $A_{sv} = cross - sectional\ area\ of\ shear\ reinforcement (mm^2)$ $f_{sy.f} = yield\ strenght\ of\ reinforcement\ used\ as\ fitments\ (MPa)$ $s = {}^{c}/_{C}\ spacing\ of\ fitments\ measured\ parallel\ to\ the\ longitudinal\ axis\ of\ a\ member\ (mm)$ $\theta_v = angle\ between\ the\ axis\ of\ the\ concrete\ strut\ and\ the\ longitudinal\ axis\ of\ the\ Member$ *and shall be taken as either* *(i)* $45^\circ or$ $(ii) chosenin\ the\ range\ of\ 30^\circ to\ 60^\circ$ $a_v = distance\ from\ the\ section\ at\ which\ shear\ is\ being$ *considered to the face of the nearest support (mm)* $f_{cv} = concrete\ shear\ strength\ (MPa)$ $f'_c = characteristic\ compressive\ (cylinder)\ strength\ of\ concrete\ (MPa)$

Table G.1- Standards provisions of shear strength (cont.)

CSA (2004)	
11.3.3 Factored shear resistance The factored shear resistance shall be determined by $$V_r = V_c + V_s$$ **11.3.4 Determination of Vc** The value of *Vc* shall be computed from $$V_c = \beta\sqrt{f'_c}\, b_w d_v$$ the term $\sqrt{f'_c}$ shall not be taken greater than 8 MPa **11.3.5 Determination of *Vs*** For members with transverse reinforcement perpendicular to the longitudinal axis, *Vs* shall be computed from $$V_s = \frac{A_v f_{yt} d_v \cot\theta}{s}$$ **11.3.6.4 General method** The value of β shall be determined from the following equation: $$\beta = \frac{0.4}{1 + 1500\varepsilon_x} \cdot \frac{1300}{1000 + S_{ze}}$$ • For sections containing at least the minimum transverse reinforcement $S_{ze} = 300\ mm$ • Otherwise, $S_{ze} = \frac{35 s_z}{15 + a_g}$ However, S_{ze} shall not be taken less than $0.85 s_z$ $$\varepsilon_x = \frac{\frac{M_f}{d_v} + V_f}{2E_s A_s} \leq 0.003$$	Where: $a_g = specified\ nominal\ maximum\ size\ of\ coarse\ aggregate (mm)$ $A_v = area\ of\ shear\ reinforcement\ within\ a\ distance\ s, (mm^2)$ $f_{yt} = specified\ yield\ strength\ of\ transverse\ reinforcement\ (MPa)$ $f'_c = concrete\ compressive\ strength\ (MPa)$ $S_{ze} = equivalent\ value\ of\ sz\ that\ allows\ for\ influence\ of\ aggregate\ size$ $S_z =$ *crack spacing parameter dependent on crack control characteristics of longitudinal reinforcement may be taken as* d_v $\beta =$ factor accounting for shear resistance of cracked concrete $\varepsilon_x =$ longitudinal strain at middepth of the member due to factored loads $\theta =$ angle of inclination of diagonal compressive stresses to the longitudinal axis of the member

Table G.1- Standards provisions of shear strength (cont.)

EC 2 (2005)	
6.2.2 Members not requiring design shear reinforcement The design value for the shear resistance $V_{Rd,c}$ is given by: $V_{Rd,c} = \left[C_{Rd,c}k(100\ \rho_1 f_{ck})^{\frac{1}{3}} + k_1\sigma_{cp}\right] b_w d$ With a minimum of $V_{Rd,c} = [\ v_{min} + k_1\sigma_{cp}]b_w d$	Where: $V_{Rd,c} = shear\ resistance\ in\ N$ $f_{ck} = characteristic\ compressive\ cylinder\ strength\ of\ concrete\ in\ MPa$ $k = 1 + \sqrt{200/d} \leq 2.0\ ,\quad d\ in\ mm$ $\rho_1 = \frac{A_{sl}}{b_w d} \leq 0.02$ $A_{sl} = area\ of\ the\ tensile\ reinforcement\ in\ mm^2$ $b_w = the\ smallest\ width\ of\ the\ cross-section\ in\ the\ tensile\ area\ in\ mm$ $\sigma_{cp} = \frac{N_{Ed}}{A_c} < 0.2\ f_{cd} \quad in\ MPa, k1 = 0.15$ $N_{Ed} =$ the axial force in the cross section in N $A_c = the\ area\ of\ concrete\ cross\ section\ in\ mm2$ $C_{Rd,c} = the\ recommended\ value\ is\ 0.18/\gamma_c$ $v_{min} = 0.035\ k^{\frac{3}{2}} f_{ck}^{\frac{1}{2}}$ $\gamma_c = partial\ factor\ for\ concrete = 1$
6.2.3 Members requiring design shear reinforcement $V_{Rd,s} = \frac{A_{sw}}{s}\ z\ f_{ywd}\ cot\theta$	Where: $\theta =$ *angle between axis of strut, compression diagonal and the tension chord of the member in deg.* $A_{sw} = the\ cross\ sectional\ area\ of\ the\ shear\ reinforcement$ $s = the\ spacing\ of\ the\ stirrups\ in\ mm$ $f_{ywd} = the\ design\ yield\ strength\ of\ the\ shear\ reinforcement\ in\ MPa$ $z = lever\ arm\ of\ internal\ force, approximatly\ equals\ to\ 0.9\ d\ in\ mm$

Table G.1- Standards provisions of shear strength (cont.)

JSCE	
9.2.2.2 Design shear capacity of linear members The design shear capacity of a member, V_{yd} may be obtained using the following equation, $V_{yd} = V_{cd} + V_{sd} + V_{ped}$ (9.2.3) $V_{cd} = \frac{\beta_d \beta_p \beta_n f_{vcd} b_w d}{\gamma_b}$ (9.2.4) $and \quad f_{vcd} = 0.2 \sqrt[3]{f'_{cd}} \quad \left(N/mm^2\right)$ $where, \quad f_{vcd} \leq 0.72 \quad \left(N/mm^2\right)$ $if \ \beta_d > 1.5 \ then \ \beta_d = 1.5 \ then$ $\beta_d = \sqrt[4]{1000/d(mm)}$ $if \ \beta_p > 1.5 \ then \ \beta_p = 1.5 \ then$ $\beta_p = \sqrt[3]{100 p_v}$ $for \ (N'_d \geq 0)$ $\beta_n = 1 + 2M_\circ / M_{ud} \quad if \ \beta_n > 2 \ then \ \beta_n = 2$ $for \ (N'_d < 0)$ $\beta_n = 1 + 4M_\circ / M_{ud} \quad if \ \beta_n < 0 \ then \ \beta_n = 0$ Reinforcement contribution obtained by using the following eq. $V_{sd} = \left[\begin{matrix} \frac{A_w f_{wyd} (sin\alpha_s + cos\alpha_s)}{S_s} \\ + \frac{A_{pw} \sigma_{pw} (sin\alpha_p + cos\alpha_p)}{S_s} \end{matrix} \right] \frac{z}{\gamma_b}$ (9.2.6) For nonprestressed members and stirrups perpendicular to the member axis, $V_{sd} = \frac{A_w f_{wyd}}{S_s \gamma_b} z$	Where: V_{cd} = design shear capacity of linear members without shear reinforcing steel, obtained using the following eq. $N'_d = design \ axial \ compressive \ force$ $M_{ud} = pure \ flexural \ capacity \ without \ axial \ load$ $M_\circ = flexural \ moment \ necessary \ to \ cancel \ stress$ *due to axial force at extreme tension fiber corresponding to design flexural moment* M_d $b_w = web \ width, \ d = effective \ depth, p_v = A_s / b_w d \ A_s =$ $area \ of \ tension \ reinforcement (mm^2)$ $f'_{cd} = desing \ compressive \ strength \ of \ concrete,$ $in \ (\frac{N}{mm^2})$ $\gamma_b = 1.3 \ may \ be \ used \ in \ general$ $V_{sd} = design \ shear \ capacity \ of \ shear$ $p_v = tension \ reinforcement \ ratio$ *Where,* $A_w = area \ of \ shear \ reinfrocement \ placed \ in \ \boldsymbol{S_s}$ $\alpha_s = angle \ between \ shear \ reinforcement \ and$ *Member axis* $z =$ *distance from location of compressive stress resultant to centroid of tension steel, may generally be taken as d/1.15* $\gamma_b = member \ factor, generally \ be \ takedn \ as \ 1.1$ $f_{wyt} = design \ yield \ strenght \ of \ shear$ $reinforcement$

BIBLOGRAPHY

1. ACI Committee, American Concrete Institute and International Organization for Standardization, 2008. Building code requirements for structural concrete (ACI 318-08) and commentary. American Concrete Institute.

2. Aldred, J., and Day, J. (2012). “Is geopolymer concrete a suitable alternative to traditional concrete?”. The 37th Conference on Our World in Concrete & Structures 29-31 August 2012, Singapore.

3. AS 3600, A.S., 2001. Concrete structures. *AS3600-2001*. *Sydney (Australia): Standards Australia*.

4. ASCE-ACI task committee 426 (1973). “The shear strength of reinforced concrete members”. Journal of the structural division.

5. Aydin, S., and Baradan, B. (2012). “Mechanical and microstructural properties of heat cured alkali-activated slag mortars”. Materials & Design, vol. 35, pp. 374–383.

6. Canadian Standards Association, 2004. *Design of concrete structures*. Canadian Standard Association.

7. Canbay, E. and Frosch, R.J. (2005). “Bond Strength of Lap-Spliced Bars”. *ACI Structural Journal*, 102 (4), 605–614.

8. Chang, E.H. (2009). “Shear and bond behavior of reinforced fly ash-based geopolymer concrete beams”. A thesis presented to Curtin University of Technology, Perth, Australi.

9. Diaz, E.I., Allouche, E.N., Eklund, S. (2010). “Factors affecting the suitability of fly ash as source material for geopolymers”. *Fuel* 2010, 89, 992–996.

10. Foster, S.J. (2010). "Design of FRC Beams for Shear using the VEM and the Draft Model Code Approach". Bulletin No. 57, Shear and Punching Shear in RC and FRC elements, Workshop 15-16 October, Salo, Italy, pp: 195-210.

11. Hawkins, N.M., Kuchma, D.A., Mast, R.F., Marsh, M.L. and Reineck, K.H. (2005). “Simplified Shear Design of Structural Concrete Members”. NCHRP Web-Only Document 78 (Project 12-61): Contractor’s Final Report—Appendixes.

12. Japan Society of Civil Engineers, 2007. *Standard specification for concrete structure*. JSCE No. 15, Tokyo, 154–159.

13. Jeyasehar, C.A., Saravanan, G., Salahuddin, M., Thirugnanasambandam, S. (2013). “Development of fly ash based geopolymer precast concrete elements”. Asian J. Civ. Eng. 14 (4) (2013) 605–615.

14. Joseph, B., and Mathew, G. (2012). “Influence of aggregate content on the behavior of fly ash based geopolymer concrete”. Scientia Iranica A (2012) 19 (5), 1188–1194.

15. Kong, F.K. ed., 2006. *Reinforced concrete deep beams*. CRC Press.

16. Li, X., Ma, X., Zhang, S., Zheng, E. (2013). “Mechanical Properties and Microstructure of Class C Fly Ash-Based Geopolymer Paste and Mortar”. Materials 2013, 6, 1485-1495.

17. LRFD, A., 2004. AASHTO LRFD. Bridge design specifications.

18. Madheswaran, C. K., Ambily, P. S., Lakshmanan, N., Dattatreya, J. K., Sathik S. A. J. (2014). “Shear Behavior of Reinforced Geopolymer Concrete Thin-Webbed T-Beams”.

19. *ACI Materials Journal*, V. 111, No. 1.

20. Mathew, B. J., Sudhakar, M., Natarajan, C. (2013). ”Strength, economic and sustainability characteristics of coal ash –GGBS based geopolymer concrete”. *International Journal of Computational Engineering Research* Vol. 3 Issue 1.

21. McGregor, J.G., Wight, J.K., Teng, S. and Irawan, P. (1997). “*Reinforced concrete: mechanics and desig*”. (Vol. 3). Upper Saddle River, NJ: Prentice Hall.

22. McLellan, B. C., Williams, R. P., Lay, J., Van Riessen, A., Corder, G. D. (2011). “Costs and carbon emissions for geopolymer pastes in comparison to ordinary portland cement”. Journal of Cleaner Production 19-1080e1090.

23. Mourougane, R., Puttappa, C.G., Sashidhar, C., Muthu, K.U. (2012). “Shear behavior of high strength GPC/TVC beams”. Proceedings of International Conference on Advances in Architecture and Civil Engineering, 21–23 June 2012, Bangalore, India, pp. 142–145.

24. NG, T.S. (2011). “An investigation into the development of high performance geopolymer concrete”. A Thesis presented to University of South Wales, Sydney, Australia.

25. NG, T.S., Foster, S.J. (2011). “Shear strength of lightweight fibre reinforced geopolymer concrete composite beam”. Fragomeni, Venkatesan, Lam, Setunge (Eds.), Incorporating Sustainable Practice in Mechanics of Structures and Materials, Taylor & Francis Group, London.

26. No, E., 1992. 2, Design of Concrete Structures, Part 1: General Rules and Rules for buildings. *Commission of European Communities ENV*, pp.1-1

27. Sanni, S., Khadiranaikar, R. (2013). “Performance of geopolymer concrete under various curing conditions”. IJSR - International journal of scientific research (Volume: 2, Issue: 3, Mar 2013, ISSN No 2277 – 8179).

28. Sofi, M., Van Deventer, J.S.J., Mendis, P.A., Lukey, G.C. (2007). “Bond performance of reinforcing bars in inorganic polymer concrete”. (IPC), J. Mater. Sci. 42 (2007) 3107–3116.

29. Sumajouw, D.M.J., Hardjito, D., Wallah, S.E., Rangan, B.V. (2005). “Behavior and strength of reinforced fly ash-based geopolymer concrete beams”. Construction and Building Materials 120 (2016) 251–264 263 Australian Structural Engineering Conference, 11–14 September, Newcastle, Australia.

30. Vecchio, F.J. (2000). “Disturbed stress field model for reinforced concrete formulation”. J. Struct. Eng. 126 (9) (2000) 1070–1077.

31. Wallah, S. E. and Rangan, B. V. (2006). “Low-calcium fly ash-based Geopolymer concrete: long-term properties”. Research Report GC 2, Curtin University of Technology, Perth, Australia.

32. Yost, J.R., Radlinska, A., Ernst, S., Salera, M., Martignetti, N.J. (2013). “Structural behavior of alkali activated fly ash concrete”. Part 2: structural testing and experimental findings, Mater. Struct. 46 (2013) 449–462.

VITA

Noor Yacob was born in Baghdad, Iraq in 1973. She received her Bachelor degree of Civil Engineering in 1995 from Al-Mostansiriya University (Baghdad, Iraq). She began her Graduate Certificate Program in Contemporary Structural Engineering at Missouri University of Science and Technology in fall 2011 as a distance student, then proceeded to master degree, as on campus student, in spring 2013.

In the last year of her Bachelor studies, she participated as a co-up in Al-Yarmouk Hospital reconstruction project, The Double-Deck Bridge in Al-Jadiriya, and the Modern-housing of Souq-Hamada project in Baghdad, Iraq. After graduation with Bachelor degree, she worked in the Iraqi Parliament as engineer in training for the maintenance department. In December 2016, she received her Master's degree in Civil Engineering from Missouri University of Science and Technology.